

IMPERIAL COLLEGE LONDON

PHYSICS MSci PROJECT REPORT

COMPLEXITY AND NETWORKS GROUP

Applying a Simple Model of Atrial Fibrillation to a Complex, Realistic Geometry

Author's CID:
00729195

Supervisor:
Prof. Kim CHRISTENSEN

April 25, 2016

Word Count: 9586

Abstract

Atrial fibrillation, an arrhythmia of the atrium, is a prevalent disease affecting 35 million people worldwide. A number of computer models have been developed to better understand the condition, including a simple cellular automata model by Christensen *et al* which demonstrates how fibrosis, a reduction in cell connectivity, leads to the spontaneous emergence of atrial fibrillation. This report details the development of a cellular automata model which applies the same rules used by Christensen *et al* to a substrate with a realistic geometry and cell connectivity. Image based data from a sheep's atrium was kindly provided by Dr. Jichao Zhao of the University of Auckland, and significant data processing was undertaken to discretize the physiological data. This model was shown to preserve the statistical behaviour seen in the Christensen *et al* model, in particular the sharp transition relationship between the transverse coupling, ν , and the risk of AF. The model did result in new mechanisms for AF to develop, as fibrillation was shown to occur without rotors and instead as the result of wandering wavelets arising from the heterogeneous connectivity of the fibre orientation. A simple 3D model was also created by coupling together 2D sheets of the original Christensen *et al* model. The 3D geometry was shown to preserve the transition relationship between ν and risk of atrial fibrillation. Increasing the number of layers in the model was shown to shift the transition, making the system less stable for higher numbers of layers.

Acknowledgements

I would like to thank my supervisor Prof. Kim Christensen for his guidance over the course of the project. I would also like to thank Kishan Manani, PhD student in the Complexity and Networks group, for his advice and support.

Particular thanks to Dr. Zichao Zhao for sending us his data on the geometry and fibre orientation in a sheep's atrium. Without his kindness we would not have been able to carry out this project. Thank you to Dr. Chris Cantwell for his advice on the processing the dataset.

Finally, thank you to my project partner.

Contents

0.1	Summary	8
0.2	Declaration	9
1	Introduction and Theory	10
1.1	Introduction	10
1.2	Medical Theory	10
1.2.1	Medical Introduction to AF: Overview	10
1.2.2	Electrical conduction in Myocardium	11
1.2.3	Treatment Options	12
1.2.4	Current Understanding of Factors causing AF	13
1.3	Computational Theory	13
1.3.1	Current Approaches to Modelling Cardiac Dynamics	13
2	Christensen <i>et al</i> Model	16
2.1	Theory	16
2.1.1	Model behaviour and Critical structures	16
2.1.2	Analytical Results	17
2.1.3	Markov Chain Analysis	18
2.2	Implementation of Christensen <i>et al</i> Model	19
2.2.1	Parameter Fitting	19
2.2.2	2D Model Statistics	19
2.2.3	The Role of Heterogeneity	20
3	Extensions and Investigations	22
3.1	Purpose and Motivation	22
3.2	Implementation of the 3D Cylindrical Model	22
3.2.1	Implementation of Anatomical Model	23
3.2.2	Fibre Orientation	25
3.2.3	Scaling of parameters in the Anatomical model	27
3.2.4	Pacemaker cells	27
3.2.5	Computational performance and memory	27
3.3	Event Lifetime Investigation	30
4	Results	32
4.1	3D Cylindrical Model Results	32
4.2	Anatomical Model Results	36
4.2.1	Transition curve relationship	36
4.2.2	New Phenomena	37
4.3	Event Lifetime Results	40
5	Conclusion	42
5.1	Further Developments	42
6	Appendix	44

0.1 Summary

Atrial fibrillation (AF) is an arrhythmia of the atrium that causes the heart to beat rapidly and irregularly. It is a prevalent disease, affecting 35 million people worldwide. Computational models have been used to better understand this disease since the 1960's. This report details the development of a cellular automata model applied to a substrate with a realistic geometry and cell connectivity of a sheep's atrium. This model demonstrates how fibrosis, a reduction in cell connectivity, leads to the spontaneous emergence of atrial fibrillation. That relationship is explored quantitatively and the results compared to those gained by the 2D Christensen *et al* cellular automata model. A simple 3D extension of the Christensen *et al* model is also investigated to determine the effects attributable to the realistic geometry and connectivity.

Introduction and Theory:

This chapter gives an introduction to atrial fibrillation, describing the disease, its impact and its known medical causes. The current treatments for AF are outlined. An introduction is given to the types of computer models commonly used to simulate electrical transport in cardiac tissue.

Christensen *et al* Model:

This section describes the model developed by Christensen *et al* that was used as the basis for the project. The theoretical workings of the model and its analytical solutions are described. The model is re-implemented and a summary of the main results obtained is included.

Extensions and Investigations:

This chapter consists of three distinct sections. Firstly, it describes the 3D model that was developed as an extension of the Christensen *et al* model. Secondly, it outlines how cellular automata and image based models were combined to create a model based on a realistic yet discretised geometry. This model uses data of the fibre orientations in a sheep's heart obtained from Dr Zhao at the University of Auckland. Lastly, an investigation into mean lifetime of AF events and how it relates to defective cells (described by parameter ϵ) is given.

Results:

In this section the results from the two newly developed models are compared to those obtained by Christensen *et al*. Following the structure of the previous section, it consists of results from three areas: the 3D layers model, the realistic geometry model and the investigation into mean lifetime of events.

Conclusion and Further Developments:

A summary of the areas investigated and the significant results, particularly those from the realistic geometry model are outlined. Future developments given focus on the improvement and application of the anatomical model.

0.2 Declaration

Neither of the students had any prior experience working on the research area nor with the model before undertaking this project.

It should be emphasised that it was the students own idea to implement the original model (defined on a two-dimensional substrate) on a real atrial substrate in order to investigate whether new phenomena emerged. I very nearly vetoed the proposal due to the enormous work involved but I decided to let the students have a go as they were extremely enthusiastic about their proposed project.

Both students contributed equally to this work. The project pair worked truly collaboratively on most aspects of this project, and all main components of the program contain code written by both students. The original model, including the core algorithm, was formulated by Christensen et al [insert ref] but entirely implemented by the students. The students have made extensive use of open-source third party software libraries, such as numpy (for numerical routines and objects), Cython (for optimisation), matplotlib (for graphs), and Mayavi (for 3D visualisation). However, I stress once again that all of the code specific to this project has been written entirely by the project pair. The student would not have been able to complete this work without the sheep atrial dataset kindly provided by Dr. Jichao Zhao at the University of Auckland and additional advise by PhD student Kishan Manani, and Dr. Chris Cantwell.

Prof. Kim Christensen, Project Supervisor

Chapter 1

Introduction and Theory

1.1 Introduction

Atrial fibrillation (AF) is an arrhythmia that limits the heart's ability to pump effectively. It is characterised by rapid and irregular beating of the atrium and predisposes patients to a number of other medical conditions. It leads to the formation of clots and thromboemboli and is known to be the 'single most important cause of ischaemic stroke in people older than 75' [1]. According to the Global Burden of Disease study, the condition affects 0.5 % of the total population, approximately 33.5 million people worldwide, with findings suggesting that between 1990 and 2010 there has been progressive increases in the prevalence of AF-associated mortality [2]. The large societal impact of atrial fibrillation gives motivation to better understand the condition and to improve the current treatment options. Computational models show great potential to both these ends.

This report will describe the research undertaken for an MSci project that builds on the cellular automata model developed by Christensen *et al.* It will give an introduction to both the disease itself and methods by which it can be computationally modelled, including the implementation used by Christensen *et al* which linked atrial fibrillation to heterogeneity in the cardiac tissue. This report will outline the modifications made to the Christensen *et al* model that resulted in the development of two models of increased complexity and heterogeneity, namely, extending Christensen *et al*'s model into 3 dimensions and applying it to a substrate with the realistic geometry and fibre orientation of a sheep's atrium. The results from all three models will be compared to determine whether these models preserve the behaviour of the Christensen *et al* model and whether new phenomena will be observed as a result of the increased complexity.

1.2 Medical Theory

1.2.1 Medical Introduction to AF: Overview

Atrial fibrillation is a disease which manifests as irregular and rapid activation of the atrium, classified as 400-600 pulses of the atrium muscular wall in humans. The normal pacemaker of the heart, the sinoatrial node, is not in control of the rhythm and this translates to multiple activation wavefronts propagating continuously through the atrial heart tissue in a random fashion, causing the heart to quiver rather than beat and impeding its ability to pump blood effectively, as illustrated in Figure 1.1. [3]

Signals in the heart originate from the pacemakers and pass across the atria to the ventricles, causing the muscle to contract and enabling it to pump blood. Atrial fibrillation only decreases the efficiency of ventricular pumping by 20 to 30 %, allowing a patient to live for years with the condition. The patient will however demonstrate a very irregular heartbeat, with ventricular contractions varying from 0.35 to 0.95 seconds, due to impulses arriving from the atrial muscle rapidly but irregularly [4]. Patients with atrial fibrillation experience episodes of arrhythmia of varying duration which self terminate, which is known as paroxysmal AF. As the condition worsens these episodes become longer until they are continuous, at which point the patient is said to have persistent AF.

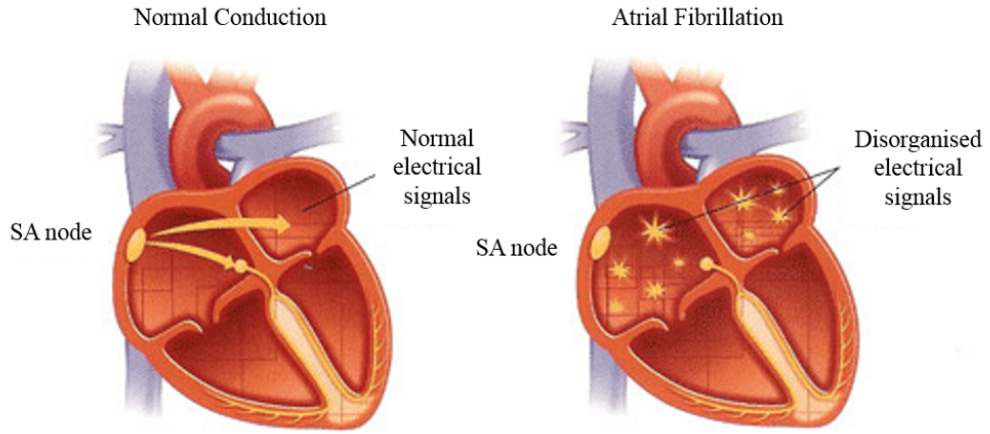


Figure 1.1: On the left: a normal heart with regular pulses being emitted from the sinus node and transmitted across the atrium in a steady fashion. On the right: irregular wavefronts across the atrium characteristic of AF. [5]

1.2.2 Electrical conduction in Myocardium

Cardiac myocytes have a length of approximately 100 um, a diameter of 25 um and are connected to each other through cell membranes known as intercalated disks. Gap junctions between cells permit the transmission of electrical impulses. The cells are arranged in myofibrils (bundles of fibre), consisting of many myofilaments [6], as shown in Figures 1.3. There are lateral connections between the myofilaments every 100 to 150 um [7]. As a result of this structure action potential propagates faster along the fibres than across them.

These lateral connections play a critical role in ensuring the electrical impulse passes smoothly through the heart. As it is biological tissue, some cells are likely to be defective and may not transmit the electrical impulse. Inter-fibrotic connections allow these cells to be bypassed, ensuring the impulse can continue to propagate along all fibres. For example, suppose the the myocyte outlined in red in Figure 1.2 is defective. Assuming an impulse coming in from the left, the second lateral connection will ensure that propagation continues along the top fibre despite the defective cell. Fibrosis is the process whereby the number of inter-fibre connections decreases; it is observed to worsen with age.

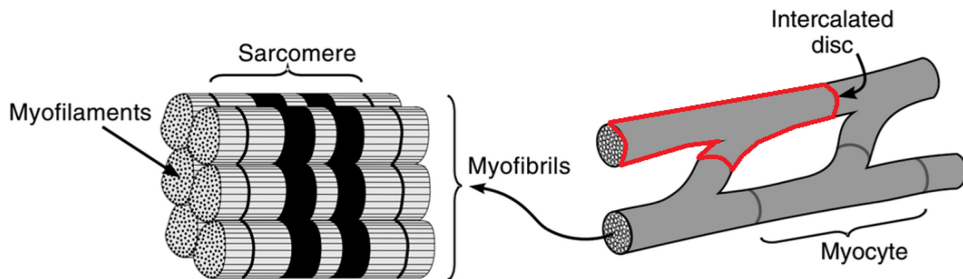


Figure 1.2: Architecture of the myocardium: individual cells or 'myocytes' are connected in long fibres with occasional transverse connections between fibres. [8]

Electrical impulses travel through the tissue by means of an action potential across cell membranes. The action potential consists of a rapid increase in the transmembrane potential (a depolarisation of the membrane) followed by a slow recovery to resting conditions, as shown in Figure 1.4. An action potential in one cell leads to action potentials being initiated in adjacent cells, allowing the electrical impulse to spread through the tissue. [9]

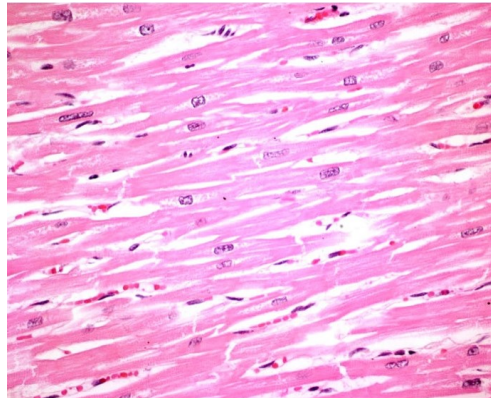


Figure 1.3: Image of stained cells in the heart muscle showing its characteristic branching structure. [10]

The electrical stimulation is typically received from an adjacent cell or pacemaker cell, and once a cell is stimulated it begins an exchange of cations and anions that form the action potential, as shown in Figure 1.4. The cell is in its absolute refractory period from section 0 up until partway through section 3, when the potential reaches a value of -60mV , in which it is impossible for an action potential to be initiated in the cell. The remainder of section 3 is the relative refractory period, in which a stronger than usual stimulus is required to initiate another action potential. [11]

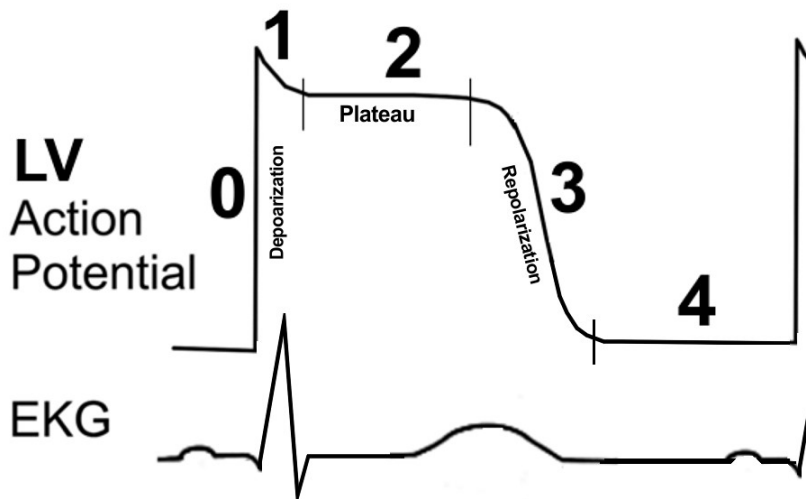


Figure 1.4: Cardiac action potential, showing the change in trans-membrane potential over time and the resulting readout from an Electrocardiogram. Upon excitation the cell is depolarized at 0, causing a spike in the EKG. After some time the cell relaxes and can be excited again by a stimulus. [12]

1.2.3 Treatment Options

Traditionally, cardiac arrhythmias can be treated with antiarrhythmic drugs that modify cardiac electric properties and thereby allow the heart rhythm to be controlled. These drugs are not specific to atrial activity and can lead to unfavorable effects on ventricular electrophysiology [13], in some cases leading to proarrhythmia and increased mortality.

In the past 15 years surgical treatments have become a favoured method of treating AF, in particular ablation therapy [14]. Ablation is a surgical procedure by which areas of atrial tissue are destroyed to prevent abnormal electrical signals from moving across the heart. Electrodes are attached to the heart during the surgery to help identify the areas which are the source of the abnormal signals. However, an inability

to identify these regions accurately has resulted in unsatisfactory clinical results. Ergo, there is scope for the accuracy of this procedure to be improved using personalised, high resolution models of the patients heart to both better understand the condition and to identify these critical regions. Computer models show similar potential for other treatments such as the Maze procedure, where the atrium is divided surgically into electrically disparate sections to prevent abnormal signals travelling across the heart [3].

1.2.4 Current Understanding of Factors causing AF

Despite the large number of patients affected by this disease the exact physiological causes of the condition are not well understood. The frameworks for understanding atrial fibrillation can be divided into three classifications: ectopic foci, single re-entrant circuits causing AF located in either atrium and lastly, 'multiple re-entry circuits with spatial and temporal variation' [3]. Ectopic foci refers to pacemaker activity in an unexpected location of the atrium. Re-entrant circuits, or *rotors*, are explained in more detail in Chapter 2.

The classification of the cause of fibrillation affects the optimal course of treatment. If caused by multiple re-entry circuits, AF is best treated with ablation or the Maze procedure. Alternatively, ectopic foci would suggest targeted ablation or drugs that suppress ectopic activity. [3]

In the last 50 years, multiple re-entry circuits have been the main model used to describe AF, partially due to the first development of a computer model of atrial fibrillation which demonstrated the influence multiple entry wavelets have on the perpetuation of AF [15]. However, in the last 5 years research has suggested that that multiple re-entry circuits do not solely explain AF [3]. Observations of AF in sheep's hearts, which possess somewhat similar physiology to human hearts, suggest ectopic foci and single re-entry circuits to be definite contributing factors [17], whilst it has been shown that single re-entry circuits help perpetuate AF in patients with congenital heart failure. Thus all three concepts are still considered potential frameworks for understanding AF.

1.3 Computational Theory

1.3.1 Current Approaches to Modelling Cardiac Dynamics

Computational models of cardiac tissue can be categorized into three types: ion channel models, cell models and tissue models. Modeling atrial fibrillation, even in the simplest mathematical form, involves the propagation of an electrical impulse (atrial cell action potential) in a network of cells. As such tissue models are of most use in describing the propagation of action potential and are outlined below. They can be separated into biophysical models that describe cell processes in detail (and are thus computationally heavy) and phenomenological models which attempt to reproduce the biological characteristics of the tissue using simpler basis rules.

Biophysical Models A mathematical formalism introduced by Hodgkin and Huxley is used as the basis of biophysical models of excitable cells, and can be used to describe atrial cell membrane kinetics such as ion currents, pumps and exchangers. The Hodgkin-Huxley model is a set of differential equations that describes the propagation of an electrical impulse through axons by modelling the cell membrane as a capacitor in parallel with an ionic current [18].

Geometric and Image Based Models The development of high resolution geometrical models, usually from scanned images, is motivated by the hypothesis that atrial fibrillation is perpetuated by specific atrial structural substrates. Surface models give a 3D representation of the atria but neglect any wall depth, unlike volumetric models [19]. Zhao et al acquired a detailed representation of a sheep heart using dissection and imaging and were thence able to deduce the effectiveness of image based models in investigating the origin of ectopic foci due to their realistic representation of atrial architecture [20]. Similarly, Macdowell et al observe the potential of personal computational cardiac models as they present a method for constructing a personalised model of fibrosis as a substrate for atrial fibrillation [21].

Phenomenological Models Phenomenological models can be described as models that are consistent with current available data but that cannot be explained using existing biological knowledge [23]. They describe phenomena more generically.

Cellular Automata Models: The simplest cellular automata model approximates cardiac tissue as a grid in which each unit exists in a number of discrete states and the state of each unit is determined

through a set of rules. Cellular automata treat time as a discrete quantity and have the advantage over biophysical models of being computationally fast.

Cellular automata models are singular in their ability to demonstrate complex macro phenomena from a basis of simple rules. This was demonstrated by Christensen *et al*'s model of AF, which used a simple grid replica of the anisotropic structure of cardiac tissue. The aim of the investigation was to provide a deeper understanding of how structural inhomogeneity can lead to the spontaneous emergence of AF. The model showed how atrial fibrillation emerged as a result of decreasing the frequency of transverse connections between cardiac fibres. In particular, the model was able to show the emergence of rotors and their dependence on wavelength and transverse connections.

Chapter 2

Christensen *et al* Model

2.1 Theory

The Christensen et al Model is a simple cellular automata model in which the cardiac tissue of the atrium is approximated as a grid. The model is discrete in both space and time.

Each unit or cell within the grid can exist in 3 distinct states, namely: excited, refractory and resting. In Figure 2.1 these are depicted in white, grey and black respectively. The state of each cell is determined by a set of rules which are as follows ¹:

- a. Any resting cell which is neighboured by and connected to an excited cell will itself become excited.
- b. All cells are connected to their neighbours in the longitudinal direction (see Figure 2.1). Some cells are connected transversally; this is probabilistic and described by the connection frequency ν .
- c. Once a cell has been excited it remains so for exactly one time step after which it becomes refractory for a period τ . During this period the cell cannot be excited, even if it shares a connection with an excited neighbour.
- d. Characteristic of a biological system, a number of the cells are defective; that is they will fail to be excited by an excited neighbour. The probability of a cell being defective is δ and in each time step its probability of failing to fire is given by ϵ .
- e. A number of cells are initialised as pacemaker cells. These aim to simulate the cells in the sinoatrial node from which the electrical impulses originate. Pacemaker cells cannot be excited by neighbours nor do they have a refractory state. Instead they are initialised as excited regularly with a period known as the firing period (T).

Periodic boundary conditions were set in the transverse direction whilst the longitudinal direction was given closed boundary conditions. Thus the topology of the model is that of a cylinder.

Biological relevance of Connection frequency ν : As portrayed in Figure 1.3, myocytes are connected to form long fibres and in a healthy myocardium these have a branching structure with fibres occasionally connected to their neighbours. This structure is mimicked in the 2D plane by a constant longitudinal frequency of 1 and $\nu < 1$. Healthy tissue corresponds to a high value of ν whilst low values of ν simulate fibrotic tissue, which has fewer inter-fibre connections.

2.1.1 Model behaviour and Critical structures

The model demonstrates that at low values of ν , the transverse connection frequency, atrial fibrillation spontaneously emerges with a high probability. This is due to the fact that decreasing ν increases the probability of critical structures forming. These critical structures are the trigger of atrial fibrillation within the model, responsible for both initiating and maintaining fibrillation. The predictions from this model can be compared to biological empirical results and thereby be used to inform ablation therapies.

At high values of ν , above 0.143 ± 0.02 , the model shows smooth wavefronts passing across the grid,

¹Please see Appendix for flow diagram of the algorithm used.

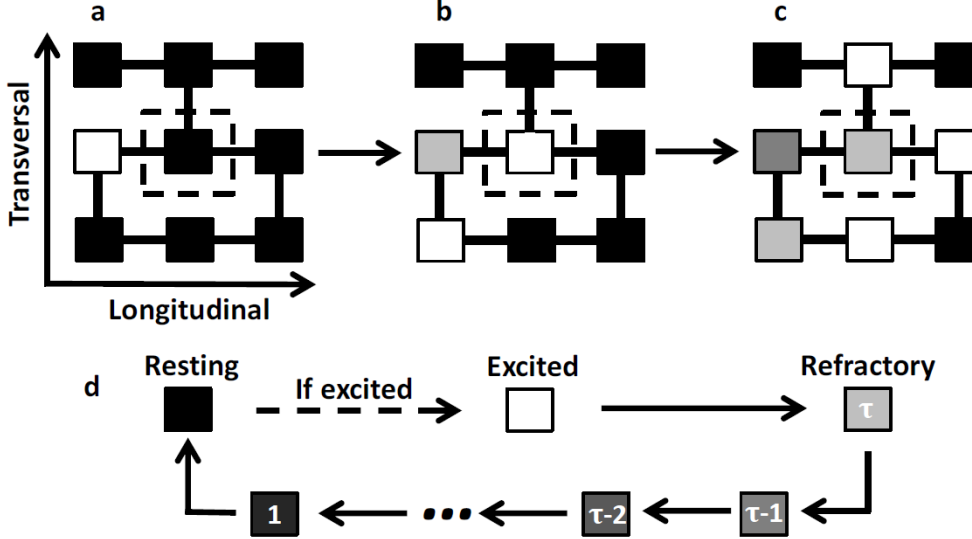


Figure 2.1: Diagram representing the rules of propagation in the Christensen *et al* model. Squares represent cells in three states: excited (white), refractory (grey) and resting (black). Figures a, b and c demonstrate the propagation of an excitatory signal across the grid. Figure d demonstrates the transitions a cell goes through once it has been excited [22].

characteristic of sinus rhythm (Figure 2.2 (a)). At values below 0.05, the defective cells erode the wavefront away as there are too few transverse connections to support conduction. However, at values of ν in the range of 0.05 and 0.143 ± 0.02 , circular wavefronts characteristic of atrial fibrillation emerge. The formation depicted in Figure 2.2(e) allows the electrical signal to form a continuous loop (depicted by the arrows), resulting in the creation of the circular wave fronts pictured in Figure 2.2(c). In this diagram the excitation is moving across the grid towards the right. Upon encountering a defective cell (outlined in red hashing), the signal is unable to continue propagating along the bottom row with a probability ϵ . However, it continues along the top row, passes down through the transverse connection and along the bottom row in the opposite direction. The signal will be able to continue propagating in a full loop, and thereby form a re-entrant circuit (or rotor), if the length between the two transverse connections is greater than $\frac{\tau}{2}$. Thus the probability of such critical structures forming is dependent upon ν , as a decrease in ν leads to an increase in the average spacing between transverse connections. The rotor will continue along this circular path until a defective cell within it fails to fire.

The circular wave fronts depicted in 2.2(c) are characteristic of fibrillatory behaviour. The frequency of these wavefronts is much higher than the firing frequency and results in the total number of excited cells in a given time step being orders of magnitude greater than the maximum number of excited cells during sinus rhythm.

2.1.2 Analytical Results

A distinct advantage of cellular automata models is that they allow for analytical solutions to be derived for the model. Christensen *et al* developed the following analytical results for both the single layer grid and a multiple layer substrate.

Let us label a cell with a vertical connection as i , and the next cell along the row with a vertical connection j . The condition for a critical structure to form is thus:

$$l_i \geq \begin{cases} \frac{\tau}{2}, & \text{for } \tau \text{ even} \\ \frac{\tau-1}{2}, & \text{for } \tau \text{ odd} \end{cases} \quad (2.1)$$

The probability of a given cell having one or more connections, p_ν is the complement of the probability of having no connections, that is:

$$p_\nu = 1 - (1 - \nu)^2 \quad (2.2)$$

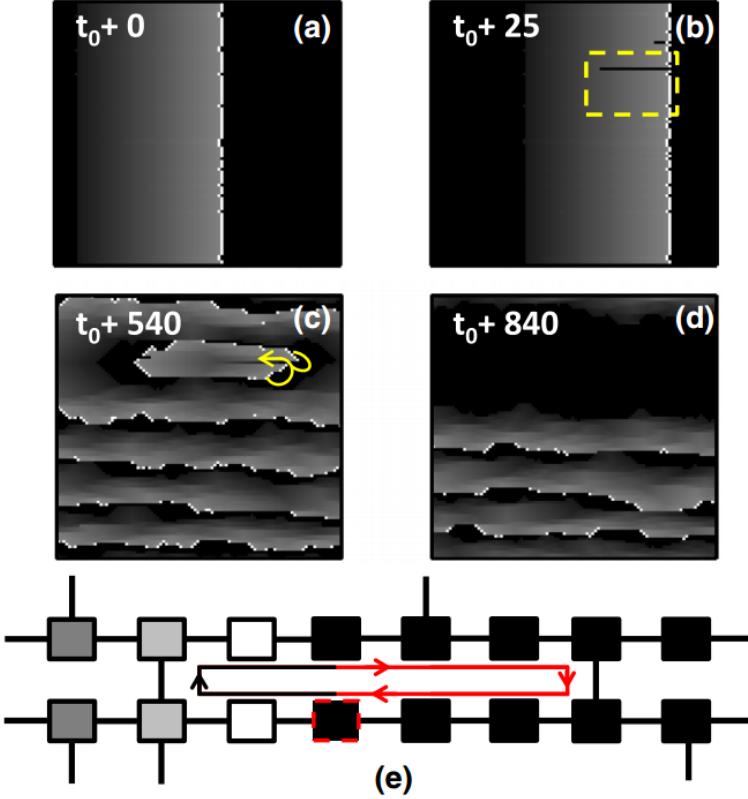


Figure 2.2: Figures (a) and (b) show a simulation of a clean wavefront characteristic of sinus rhythm in the Christensen *et al* model. A defective cell fails to fire in (b), outlined in yellow hashing, and resulting in the rotor forming in (c). Figure (e) shows the critical structure required to form a rotor, with the defective cell outlined in red hashing [22].

The probability that this dysfunctional cell, at position i , does not belong to a re-entrant circuit is thus given by:

$$P(l_i \leq \frac{\tau}{2}) = \sum_{l_i=0}^{\frac{\tau}{2}-1} p_\nu(1-\nu)^{l_i} = 1 - (1-\nu)^\tau \quad (2.3)$$

Given that the total number of cells is δL^2 , the probability that the grid has at least one such structure is given by Christensen *et al* [24] as:

$$P_{risk} = 1 - [1 - (1-\nu)^\tau]^{\delta L^2} \quad (2.4)$$

Which is the quantified risk on atrial fibrillation occurring in a given simulation. This equation can be generalised to the 3 dimensional case, which is treated as a number of 2D sheets coupled together. In this case P_{risk} is given by:

$$P_{risk} = 1 - [1 - (1-\nu)^{\frac{3}{2}\tau}]^{2\delta L^2} [1 - (1-\nu)^{2\tau}]^{(w-2)\delta L^2} \quad (2.5)$$

Where w is the number of layers [8].

2.1.3 Markov Chain Analysis

Manani [24] showed that Markov chain analysis can be used to calculate the mean time of AF events. In his analysis, the state of the chain at time t is given by the number of active cells in the system, N_A . An active cell is defined as one which is part of a wavefront originating from a re-entrant circuit. An inactive cell is one which is not part of such a wavefront, but can be. The number of inactive cells is given as N_B . This analysis looks at how the number of active particles changes over time. To calculate this, one needs to determine the transition matrix, P_{ij} , which gives the probability of the system going from i active cells to j active cells in one time step. Thus, the rate that an inactive cell becomes active, p , and the rate that an

active cell becomes inactive, q is given by:

$$p = \begin{cases} \frac{\epsilon}{T}, & \text{if } N_A = 0 \\ \frac{\epsilon}{\tau}, & \text{if } N_A \geq 0 \end{cases} \quad (2.6)$$

$$q = \frac{\epsilon}{\tau} \quad (2.7)$$

The transition matrix P_{ij} can then be calculated. In the general case it is given by the sum over the joint probability of k active cells becoming inactive with a corresponding term describing $N-j+k$ inactive cells becoming active. Thus the probability of a state going from i to j active particles is given by the binomial distribution $B(N;n,p)$, as the probability of n successful Bernoulli trials out of N trials where the probability of success is p .

$$P_{ij} = \sum_k B(i; k, q) B(N - i; j - i + k, p) \quad (2.8)$$

[24] However, in the Christensen *et al* model, for a single rotor forming this is greatly simplified as there are only 4 possible transitions a cell can make between the states 0 (having no rotors) and 1 (having a rotor) as shown in Figure 2.3. The probabilities of these are given in Equation 2.9.

$$P_{ij} = \begin{bmatrix} 1 - \frac{\epsilon}{T} & \frac{\epsilon}{T} \\ 1 - \frac{\epsilon}{\tau} & \frac{\epsilon}{\tau} \end{bmatrix} \quad (2.9)$$

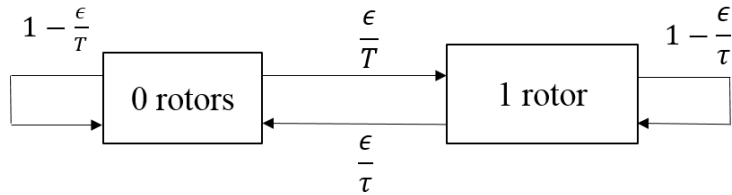


Figure 2.3: Visualisation of the four possible transitions in a Markov chain and their probabilities.

2.2 Implementation of Christensen *et al* Model

2.2.1 Parameter Fitting

Values for the parameters described above were calculated by scaling the relevant biological quantities. The average myocyte in the atrial wall has an approximately cylindrical shape, with a length of $l = 100 \mu\text{m}$ and a radius of $r = 10 \mu\text{m}$. The average area of a human atrial wall is approximately $L \times L = 20 \text{ cm}^2$. The refractory period of a cell is $\tau = 150 \text{ ms}$, much greater than $t = 0.6 \text{ ms}$, the time taken for it to depolarise. Translating these biological values into the square grid of the model gives a length $L = \frac{l}{\tau} = 1000$ cells. The grid in Christensen *et al*'s model was initialised with a length of 200 cells, giving an area of $L \times L = 40000$ unit area. This corresponds to a coarse graining factor of 5. It is necessary to keep the conduction velocity in the model equal to its biological value of approximately $\frac{l}{t} = 0.2 \text{ ms}$. In doing so, the refractory period is calculated as $\tau = \frac{\tau}{(b*t)}$. Likewise the firing frequency of the pacemaker cells is given by $F = \frac{F}{(b*t)}$, where $F = 660 \text{ ms}$, resulting in a pacing period of 220 time steps. The fraction of cells which are dysfunctional was initialised as $\delta = 0.05$, with the probability of it failing to fire also set to 0.05.

2.2.2 2D Model Statistics

The Christensen *et al* model was implemented and results compared to those in the original paper to ensure it had been implemented correctly. Amendments were then made to this model (detailed in the following chapter) to produce the original results of the project.

Figure 2.4b shows the statistics gathered from an implementation of the 2D Christensen et al Model. Each data point represents the mean time spent in fibrillation across over 100 simulations. The error bars are

calculated as the variance on the N=100 dataset. The results are in good agreement with both those collected by Christensen/Manani, plotted in red.

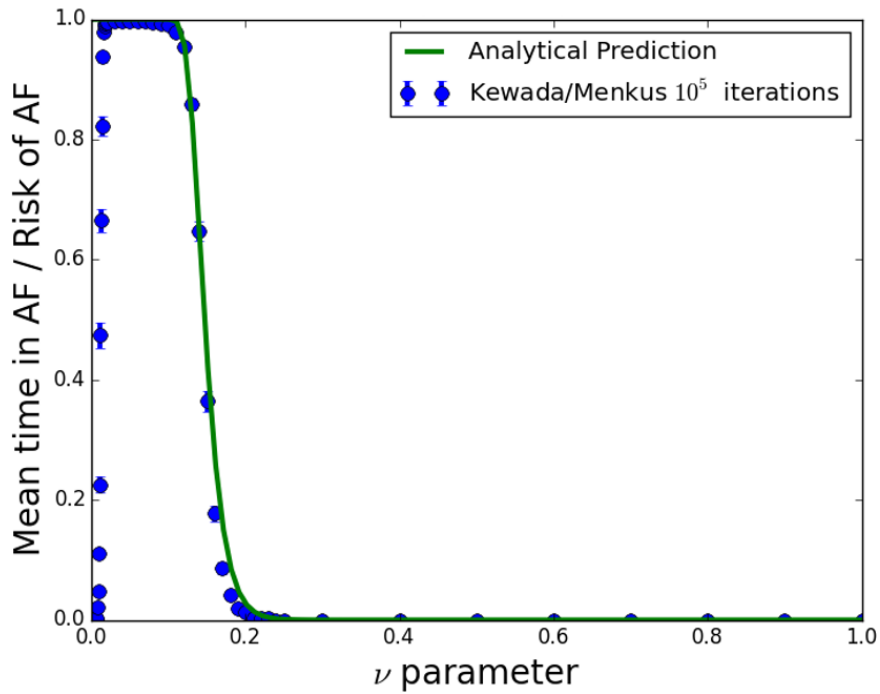
The transition curve is steepest at $\nu = 0.143 \pm 0.002$, where the error is given as the resolution of the collected datapoints. As shown, at values below 0.05 (approximately $\frac{1}{L}$, where L is the system size) the AF risk falls to zero. This corresponds to the values of ν which allow defective cells to erode away at the wave-front at a rate sufficient enough that even sinus rhythm is not supported.

Simulations run at values of ν from 0.05 up to 0.2 showed the formation of re-entry circuits triggering fibrillatory behaviour. This was verified through visualisation of the simulation.

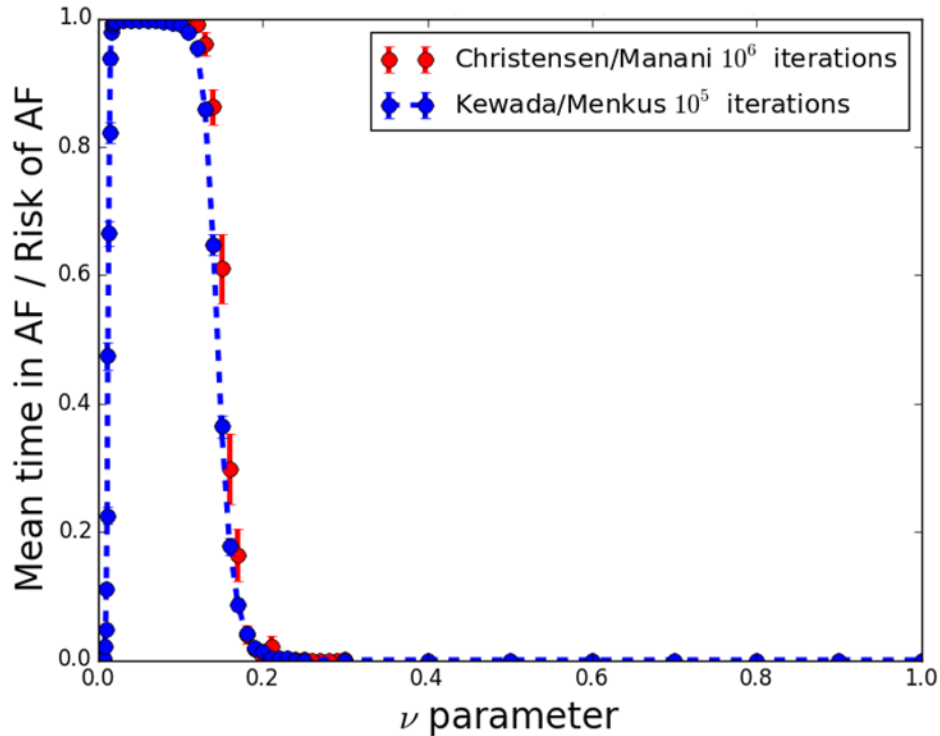
2.2.3 The Role of Heterogeneity

In essence, the Christensen *et al* model demonstrates how structural inhomogeneity leads to the spontaneous emergence of atrial fibrillation. This has been mathematically demonstrated by Greenberg and Hastings, who showed that inhomogeneities in excitable media produce stable spatial patterns that oscillate in time [27]. In particular, they observed that the patterns which emerge depend on the ratio of the number of refractory states to excited states.

Heterogeneity in the electrophysiology of cardiac tissue, as well as the structure, has been linked to the formation and perpetuation of multiple reentry circuits [25]. In particular, breaks in wave fronts have been shown to result in the spatiotemporal patterns that cause arrhythmia, validating Christensen *et al*'s result. These wave breaks may be caused by spatially fixed heterogeneities. Such anatomical obstacles tend to be unproblematic in healthy tissues, where the size of the heterogeneities are very small when compared to the width of the wavefront. However, they are able to block propagation in diseased tissue where large patches of cell death have occurred. Bub and Shrier's investigation into this phenomenon found that spiral wave activity resulted when the heterogeneities were intermediate in size (just too small to block propagation) [25]. However, these studies do not take into account heterogeneity that is inherent in the atrium from its irregular geometry and the fibre orientations of cell connectivity. The implementation of such a model is the main focus of the following chapter.



(a) Graph comparing the simulation results to the analytical solution.



(b) Graph comparing the simulation results to those collected by Christensen *et al.*

Figure 2.4: Graph showing the mean time in AF, P_{risk} , plotted against ν for a lattice of 200x200 cells, at a refractory period of 50.

Chapter 3

Extensions and Investigations

3.1 Purpose and Motivation

The 2D grid model developed by Christensen *et al* is elegant in that despite its simplicity it results in the emergence of complex macroscopic behaviours which agree with empirical trends. The two revisions to this model developed over the course of this project increase both the complexity and the level of heterogeneity within the model. Over the course of this report, ‘3D Cylindrical model’ will refer to the extension of the 2D grid into three dimensions by coupling together several 2D sheets. Similarly, ‘Anatomical model’ will refer to applying the cellular automata rules to a realistic, yet discretised geometry and simulating the flow of electrical impulses across this geometry using realistic fibre orientations.

The aim in developing such models was to determine whether they would retain the characteristic behaviours of the original 2D simulation, despite their structural differences and increased levels of heterogeneity. These characteristic behaviours include, but are not limited to, the following characteristics:

- a. The creation of the same critical structures that give rise to re-entrant circuits
- b. A qualitatively similar relationship between the transverse connection frequency ν and the risk of atrial fibrillation (a transition curve)
- c. A value of ν below which conduction is not supported in the model
- d. Detection of paroxysmal fibrillation which develops into persistent fibrillation over the course of a simulation.

The retention of these behaviours in more complex models would serve to validate the results garnered from the simple 2D model. However, the second aim of applying the model to a more realistic and heterogeneous structure was to observe any new phenomena analogous to biological behaviour.

It has been shown that reduced cell connectivity and propagation velocity (results of fibrosis) coupled with asymmetries in cell connectivity or spacing, can cause unstable propagation [25]. This research motivates the development of the Anatomical model, which can be used to show the effect a realistic, heterogeneous geometry will have on AF. The Anatomical model is essentially a hybrid: both an Geometric and Phenomenological model. This is implemented with the aim of acquiring the accuracy of a geometric model whilst benefitting from the computational speed of a cellular automata.

3.2 Implementation of the 3D Cylindrical Model

The 3D Cylindrical model was implemented by coupling together several 2D sheets. The transverse connection frequency ν was defined globally as both the intra-planar and inter-planar transverse connection frequency. As in the 2D model, periodic boundary conditions were set in the transverse direction whilst the longitudinal direction was given closed boundary conditions. The resulting topology is a cylinder with a finite thickness. A majority of the parameter values were kept consistent across the 2D and 3D models: refractory period $\tau = 50$, firing period $F = 220$, fraction of defective cells $\delta = 0.05$, probability of a cell failing to fire $\epsilon = 0.05$. Simulations were run on grids of varying thickness, from 2 layers up to a maximum of 20. The pacemaker cells were initialised as the first row in the y direction on each layer of the model.



Figure 3.1: Diagram showing the coupling together of 2D sheets to create the 3D model.

3.2.1 Implementation of Anatomical Model

This model applied the real anatomical geometry of the atrium and its fibre orientations to the Christensen *et al* model with the aim of seeing if characteristic behaviour was preserved. The geometric and fibre orientation data was obtained following correspondence with Dr Jichao Zhao in the University of Auckland, author of “An Image-Based Model of Atrial Muscular Architecture Effects of Structural Anisotropy on Electrical Activation”. Dr Zhao developed an image based model of a sheep’s atrium, including all the fibre orientation information, using serial surface imaging. The sheep’s atrium was planed at intervals of = 50 micrometres

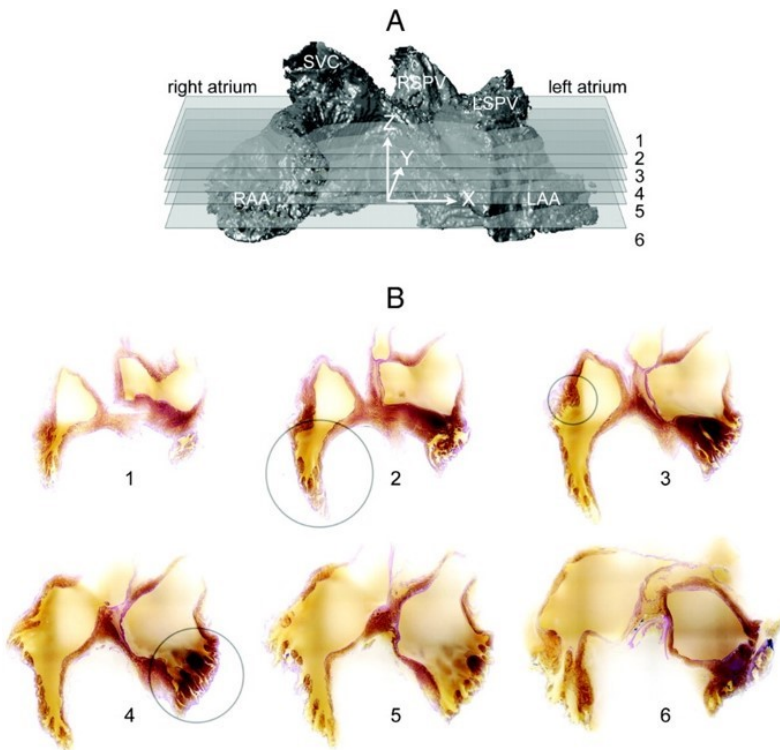


Figure 3.2: Image showing the process undertaken to Dr Zhao to obtain a volumetric model of the atrium. Figure A shows the cross-sectional slicing applied to the atrium. B shows a number of cross-sectional slices where the fibre orientation is indicated by the colour spectrum. [20]

and images of the cross-section were taken at a resolution of $50 \times 50 \times 50 \mu\text{m}^2$ to compose the volumetric model. The local myofiber orientation was obtained through eigen-analysis of the structure tensor. Given that the average dimensions of a myocyte is $100 \mu\text{m}$ by $20 \mu\text{m}$, the resolution of the data is at the order of cellular level, however, each data point does not correspond to a single cell [?]. This data was obtained as three cubic arrays (x, y, z), with the value at each index within each cube representing the magnitude of the fibre vector in a particular cardinal direction. This data represented a vector field of the myofiber orientation at discrete points in the atrial geometry. The overall magnitude of the vectors within this dataset were found to have no biological significance, and for the purpose of this model the vector field was normalised. This allowed for a geometric model to be constructed, as shown in Figure 3.4b. Once this dataset was obtained, there were two main challenges in implementing the model. Firstly, the data itself was physiological, that is, un-normalised and continuous. It had to be parsed into a discretised format in order for it to form the basis of a cellular automata model. The challenge was to do so without losing the integrity of the anatomy

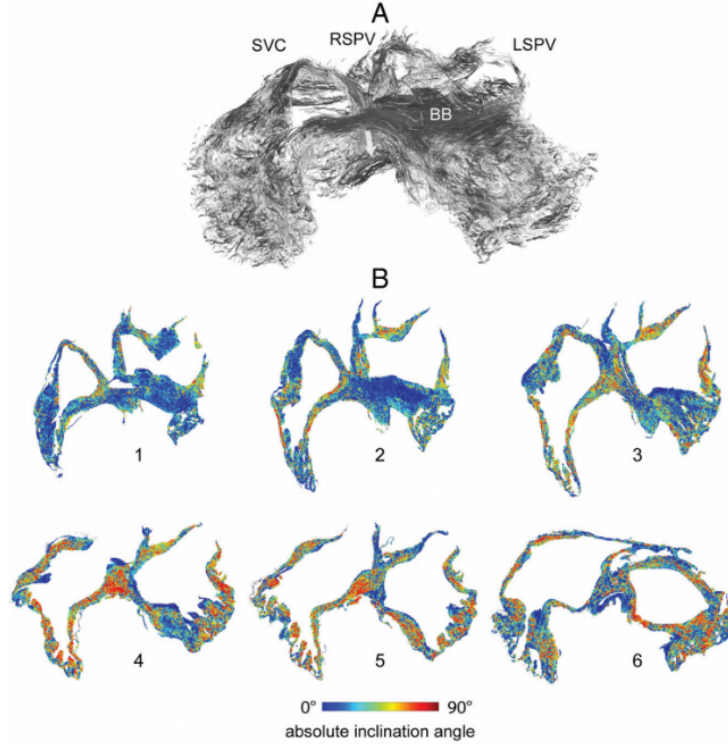
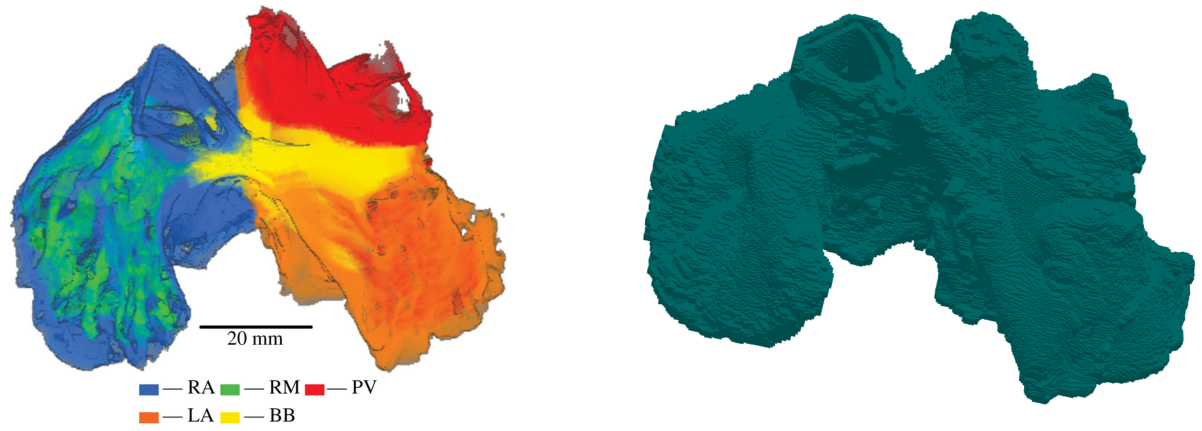


Figure 3.3: Image showing myofiber orientation within A) the full atrium of a sheep B) several crossections of the atrial chambers. The intensity of the greyscale in Image A is used to emphasize fibre orientation. The colour map in Image B is used to signify the inclination of the fibre orientation to the X-Y plane of the cross-section. [20]



(a) Dataset used to create volumetric model of a sheep atrium, as visualised by Dr. Zhao in his paper. [20]

(b) Volumetric cellular automata model of a sheep's atrium, created from the data visualized in (a).

Figure 3.4: Images showing original dataset (a) and the cellular automata model based on it (b).

it described. The second challenge was computational. The dataset was very large (4 GB): it could not be processed at once with the typical RAM of a desktop computer and runtimes on processing it were unrealistic. However, the aim was to create a model that runs considerably fast on a desktop computer as this would give impetus for the clinical applicability of image based, cellular automata models to be assessed.

The model was originally constructed as a single layer 2D surface of the heart living in 3D space. The

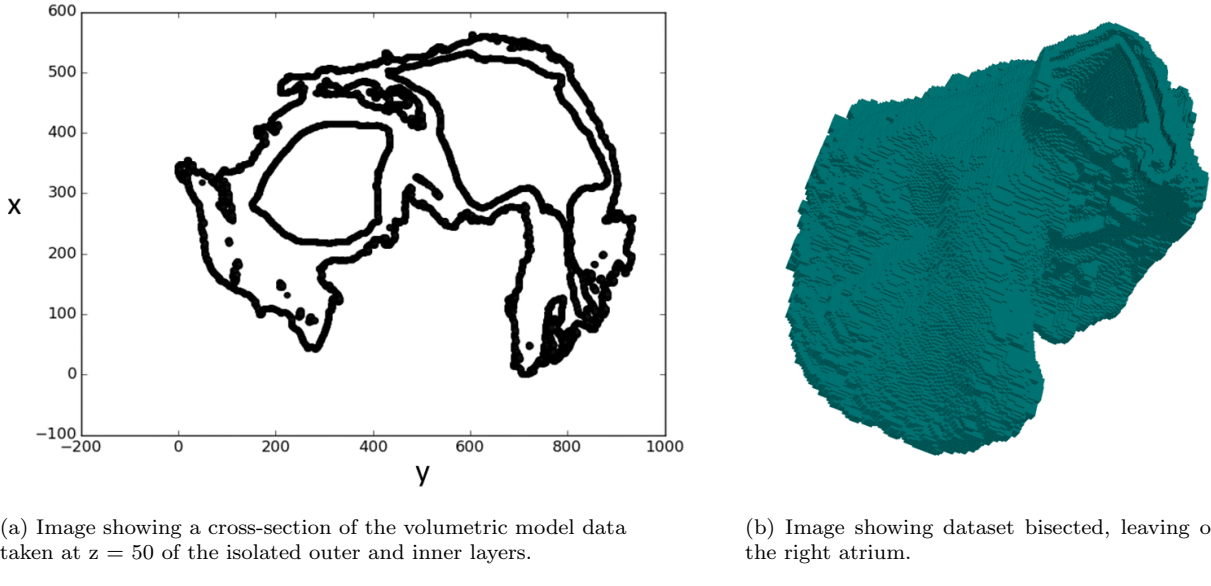


Figure 3.5: Methods undertaken to improve computation efficiency by reducing the number of cells in the substrate.

outermost layer of the data was isolated using an algorithm that identified all cells with a non-zero fibre vector which had at least one neighbouring empty cell. This gave the resulting data pictured in Figure 3.5a. Multiple surface layers of data were obtained by shaving the outermost layer off the data set, and reapplying the original algorithm to obtain the 2nd surface layer. The data was also bisected to allow for the model to be run on the right atrium alone.

3.2.2 Fibre Orientation

In order to apply this physiological data to a cellular automata model, the fibre direction had to be quantised. This was achieved by taking the dot product of the vector with each of the cardinal directions and assigning the vector to the direction for which this product has the highest value. This is pictured in a 2d plane cross-section in Figures 3.7a and 3.7b.

Using three cardinal directions to quantise the fibre orientation proved insufficient to sustain conduction. Preliminary results with this model showed that conduction could not be sustained in the model, despite high values of nu . These preliminary results showed that at values of nu less than 0.7, conduction was not supported across the atrium and basic sinus rhythm could not be sustained.

It was surmised that this issue was encountered in the single layer model due to two distinct reasons. The larger issue was assumed to be the staircase problem, which is pictured in Figure 3.6. Many cells adjacent to each other in the single layer model were observed to be in a configuration such that they were only connected to neighbours diagonally, and as a result no propagation was possible.

The second reason for low conduction was that the connections to neighbours are based upon anatomical fibre orientation that is inherently designed to work in 3 dimensions. Thus, isolating the model to a single layer is problematic for two reasons. Firstly, some of the cells are likely to have fibre directions

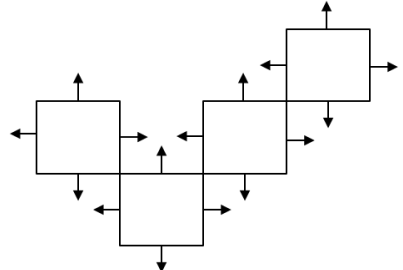
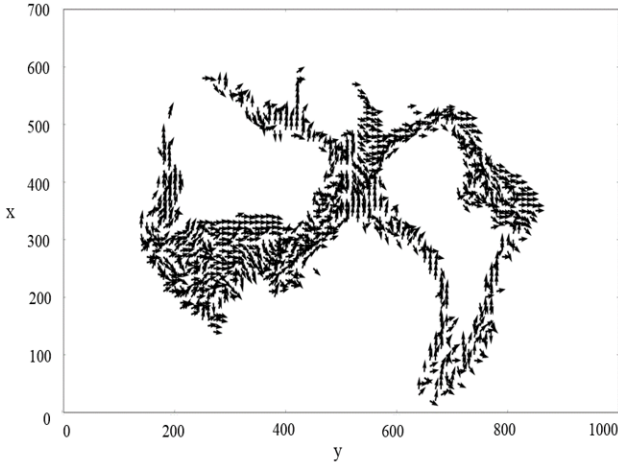
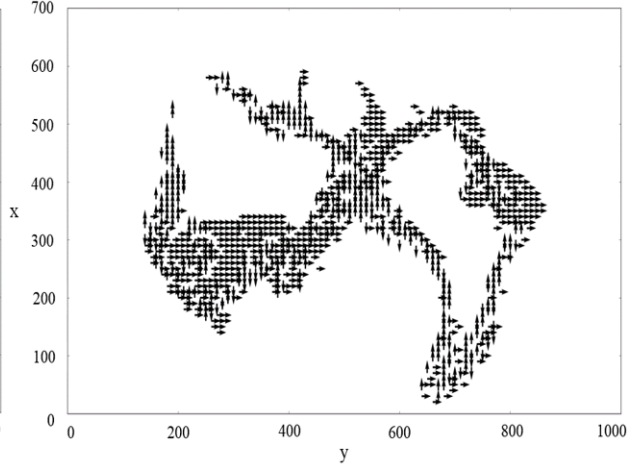


Figure 3.6: Diagram showing the ‘staircase problem’ encountered with a single layer. Cells in the single layer model were often arranged as shown, thus a total of 6 quantized directions is not sufficient to sustain conduction across the substrate.



(a) Cross-section of the original vector field representing fibre orientation.



(b) Cross-section of the vector field representing fibre orientation after being discretised to the 6 cardinal directions.

Figure 3.7: Cross-sections of the vector field before and after quantization, coarsegrained by a factor of 10 for visualization purposes.

pointing inwards which will result in them having no neighbours in the single layer case. Secondly, defective cells are more likely to halt conduction in a fibre orientated model than in the original configuration. These effects were deemed sufficient motivation to implement a several layer anatomical model.

As a result, a number of additional propagation directions were added to each cell, (effectively allowing the fibre vector to be quantised more accurately). As shown in Figure 3.8, diagonal connections were im-

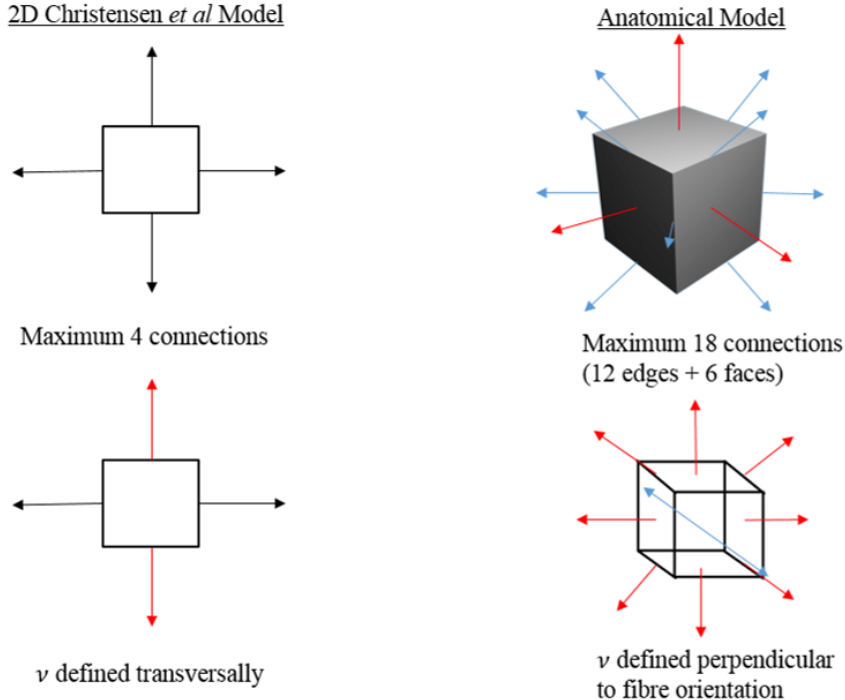


Figure 3.8: Diagram showing the maximum number of connections per cell and the definition of transverse connections for the Christensen *et al* model (left) and the anatomical model (right).

plemented and the maximum number of propagation directions was increased to 18. This increased the

complexity of the base algorithm calculating the states of cells significantly more complex. Transverse connections affected by ν were redefined to be the connections perpendicular to the fibre vector for that cell. This definition is representative of the fibre architecture seen in myofibrils.

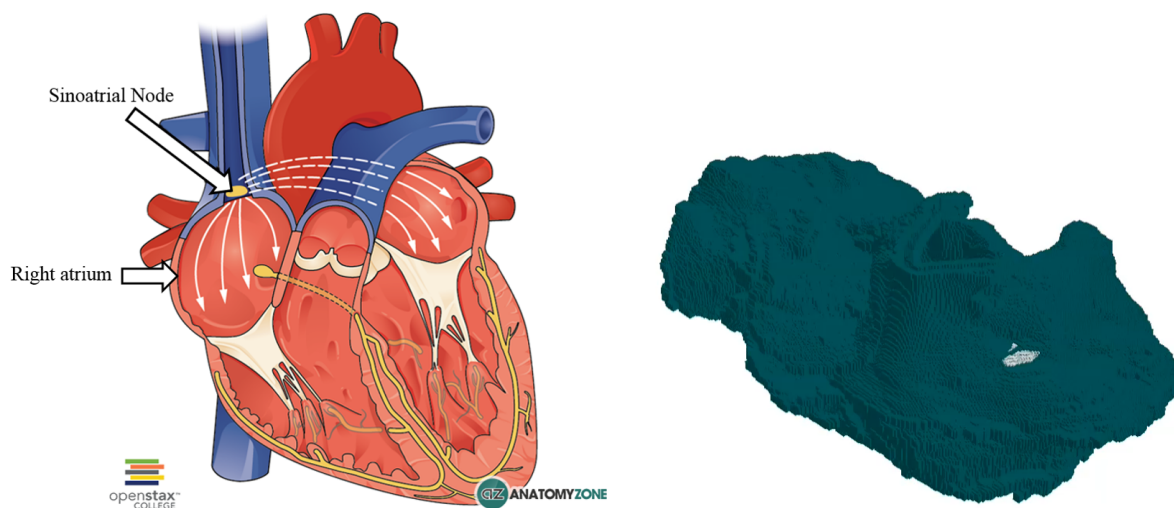
3.2.3 Scaling of parameters in the Anatomical model

The values of all the model parameters, in particular the refractory period τ and firing frequency F , had to be scaled to the new geometry. The correct values cannot be obtained from a simple analytical calculation, given the highly irregular geometry. Thus the new parameters were calculated, preliminary simulations were run using these values and small adjustments were made based on the behaviour of the model.

The parameters firstly had to be scaled by a factor of 2.5, as this is the factor by which the number of cells increased (for the single layer dataset). The conduction velocity of the signal propagation would also have increased due to the extra diagonal connections. Thus an extra scaling factor of 1.4 was applied to the original model parameters. This gave a multiplying factor of $\frac{2.5}{1.8} = 1.8$, giving a refractory period of 90 and a firing period of approximately 400.

3.2.4 Pacemaker cells

Anatomically the pacemaker cells reside in the sinoatrial node, which sits on the upper part of the right atrium wall, near the sinus venosus (the large quadrangular cavity at the top of the atrium). This location was roughly identified in the anatomical model, with the aim of initializing conduction from this location.



(a) Physiological diagram showing the location of the sinoatrial node. [26] (b) Pacemakers initialised in original model, shown in white.

Figure 3.9: Images showing the location of the pacemaker cells.

3.2.5 Computational performance and memory

Computational efficiency was a major consideration and challenge in the development of the Anatomical model. The total number of cells increased from 40 000 in the original 2D model, to 2 000 000 in the anatomical model, whilst the number of computational steps per iteration increased vastly from the additional connections for each cell. This resulted in the runtime of the model becoming unfeasible and as such, optimization became a priority. As a result, a number of optimization strategies were undertaken.

Profiling: The code was profiled in detail to identify the most computationally expensive operations. Logic changes were then implemented to optimize the algorithm.

Course graining: The data was course grained by a factor of 3, resulting in a 9 fold reduction in the size of the data set.

Data structure: The original data structure used for the vector field was a 4 dimensional array spanning the entire volume of the model. However, a vast majority of the array was white space and it was thus an inefficient use of memory. The data structure was thus transformed into a linked list, where the first three indices of each term in the list was a position vector and the next three was the propagation vector at that point. Whilst this removed the empty space, and vastly reduced the memory usage, it created the problem that the entire list had to be searched in order to determine the neighbours of each cell. This search was carried out once for the dataset, and the list index of the neighbours for each point were appending to that cells array of information. The resulting data structure was thus a 2 dimensional list, in which each term was a list containing all the information of a cell such as its position vector, whether it is defective, its connections, the indices of its neighbours etc. This data structure reduced the memory usage by 96%.

Other: Full static typing and array buffer typing were implemented in the model. Array indexing was carried out numerous times within the program and thus efficient array indexing was also implemented. Bounds checking in the compiler were disabled and the compiler settings were checked to ensure they optimised the code.

Overall, optimization resulted in a 99.8% decrease in runtime for the Anatomical model.

AF algorithmic checks

In the simulations run using the 2D and 3D Layer models, atrial fibrillation was identified using a threshold check on the total number of excited cells in a given timestep. This threshold, t_{af} was set using equation 3.1.

$$t_{af} = \alpha \frac{(L_y)^2}{F} \quad (3.1)$$

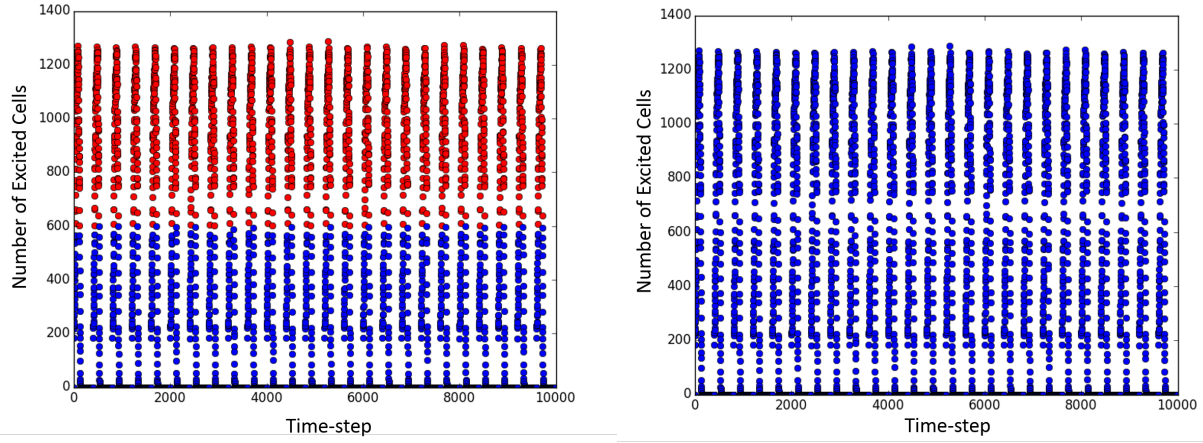
Where $\frac{(L_y)^2}{F}$ gives the number of excited cells expected on the grid during sinus rhythm and α is a scaling factor used to set a buffer. In all simulations α was set to a value of 1.5.

This simple threshold check was very successful in the 2D and 3D Layer cases, where the threshold can be calculated analytically from the system parameters and the number of excited cells during afibrillation is vastly higher than during sinus rhythm. However, this was not the case with the Anatomical model, as the number of cells excited during sinus rhythm is dependent upon the irregular geometry and the number of excited and As a result two other fibrillation checks were developed.

Moving average check: The Moving average of the number of excited cells is calcated over a period of time less than the firing period of the pacemaker cells. If this moving average is about a set threshold value, the system is deemed to be in fibrillation. The threshold value is set empirically from a number of simulations. The disadvantage of this check is that the threshold value must be redetermined when parameter values of the system are changed.

Zero check: This check works on the assumption that if the system is in sinus rhythm and the firing period is longer than the time taken for a wavefront to traverse the system, then the number of excited cells will periodically return to zero. Thus, if the number of excited cells has not been zero for a time longer than the firing period, the system is deemed to in in fibrillation.

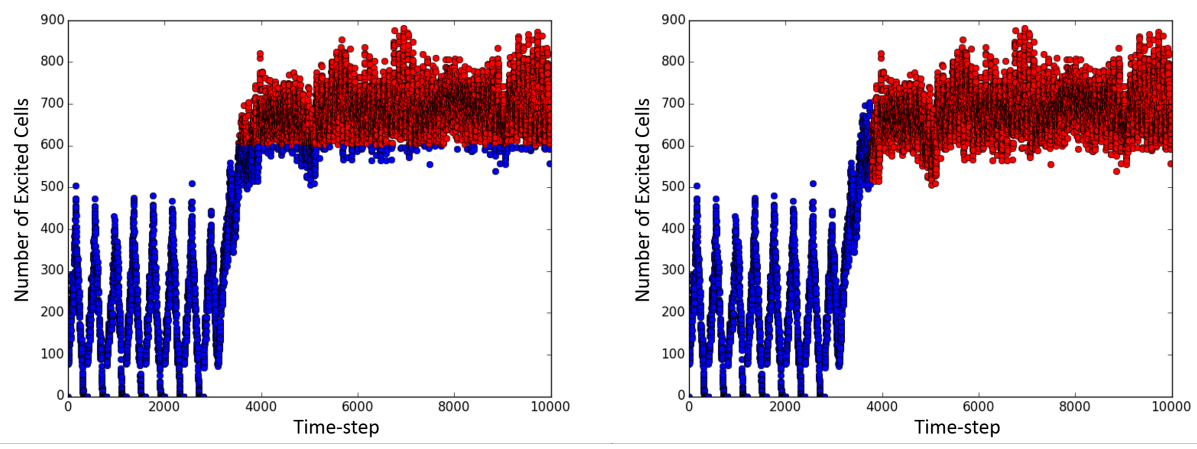
The effectiveness of these checks are demonstrated in figures 3.10 and 3.11. The data points depicted in red denote those time steps which the algorithm determined the system was in fibrillation, whilst the blue data points are time steps where the system is determined to be in sinus rhythm. As evident in Figures 3.10a and 3.11b the hard threshold check failed when applied to the Anatomical model.



(a) Hard threshold check applied to sinus rhythm.

(b) Zero check applied to sinus rhythm

Figure 3.10: Graphs showing number of excited cells over time during sinus rhythm in the Anatomical model. Datapoints classified as in fibrillation by the check are red, whilst those classified as sinus are blue.



(a) Hard threshold check applied to a fibrillating system.

(b) Zero check applied to a fibrillating system.

Figure 3.11: Graphs showing number of excited cells over time during fibrillation in the Anatomical model. Datapoints classified as in fibrillation by the check are red, whilst those classified as sinus are blue.

3.3 Event Lifetime Investigation

The probability of a defective cell failing to fire, ϵ is directly related to the lifetime of a rotor. For a single rotor the mean lifetime of events would simply scale with ϵ : a defective cell in the orginal pathway of the rotor must fail for the rotor to be terminated. As detailed in Chapter 2, a Markov chain analysis can be used to give an analytical solution to the mean event lifetime. This investigation aims to determine whether that is a good description of the phenomenon as it occurs in the model or whether higher order effects will be significant.

This investigation relied on just a single rotor being present on the grid. Thus a critical structure was hard coded into the implementation of the 2D Christensen *et al* model, and ν was set to a value of 0.9 to ensure that the probability of another rotor forming was negligible. The ϵ parameter was then varied between values of 0.01 and 0.1.

Chapter 4

Results

4.1 3D Cylindrical Model Results

The 3D Cylindrical model was found to preserve the transition curve relationship between ν and 'Risk of AF' produced by the 2D Christensen model (see Figure 2.4b). This was verified for up to a maximum of 20 layers. An example of such a result is demonstrated in Figure 4.1 which shows a sharp transition at $\nu=0.098 \pm 0.002$ for the 2 layer case and $\nu=0.112 \pm 0.002$ for the 7 layer case.

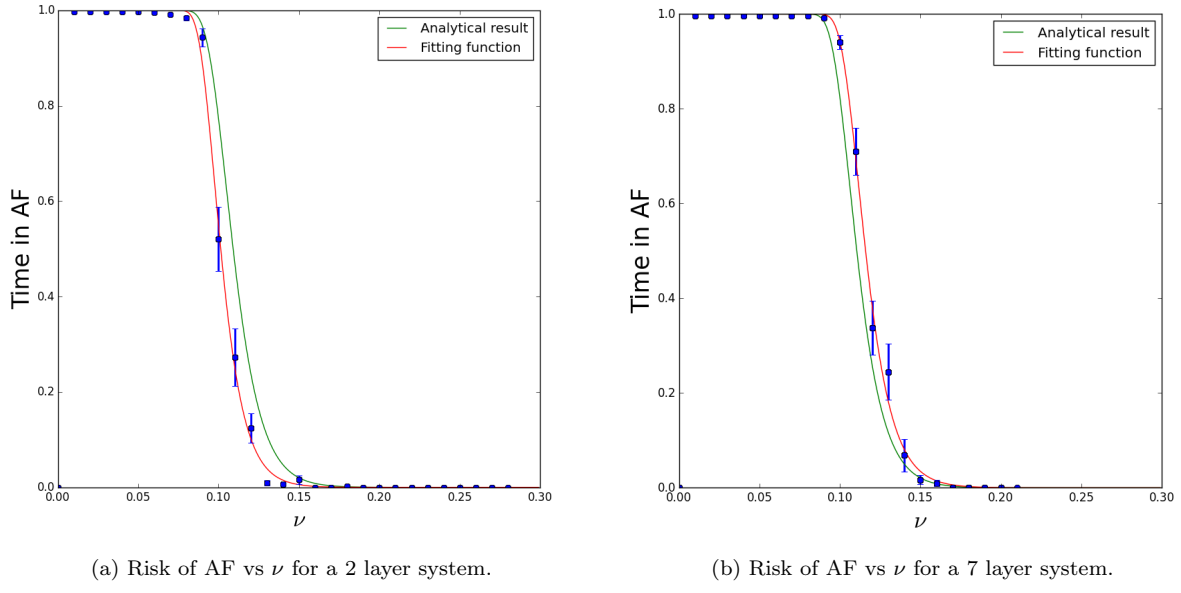


Figure 4.1: Examples of transition curve in the 3D Cylindrical Model. The transition, plotted in red, shifts higher from 2 to 7 layers. Data is taken from simulations run on a 200x200 size lattice, with $\epsilon=0.05$, $\delta=0.05$, $\tau=50$.

High levels of association were seen between layers in the model. This is demonstrated most effectively in Figure 4.2, which shows a rotor forming on the second layer and passing through the other layers. The resulting fibrillation pattern is almost identical on each layer. This result validates the hypothesis that atrial fibrillation behaves effectively as a surface phenomenon.

The extension of the model into three dimensions was shown to shift the critical value of ν at which the transition takes place. The trend of this phenomenon is summarised in Figure 4.3 which shows the steepest point of the transition for simulations run on grids of varying thickness. For a given number of layers, a set of transition data as shown in Figure 4.1. Data was gathered in increments of ν of 0.01 over the set of ν values that comprise the transition. The steepest point of each transition was calculated by fitting a function to that data and calculating the steepest point using finite difference methods.

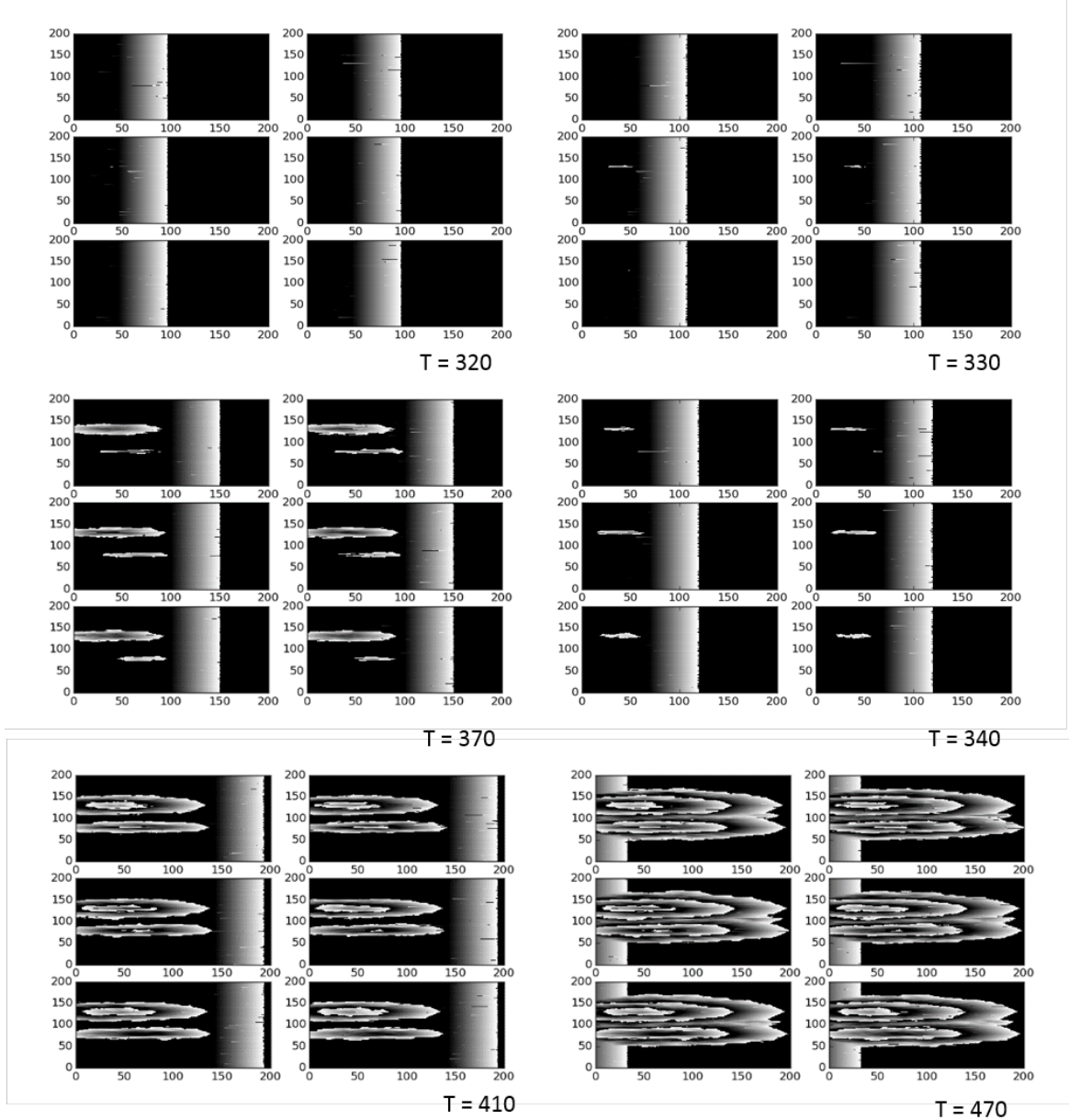


Figure 4.2: Screenshots showing the formation of a rotor in a 6 layer simulation of the 3D Cylindrical model. Layers are pictured as subplots, from left to right. Timestamps of each screenshot is given in the bottom left corner. Images show the formation of a rotor on the second layer at $T=320$ that results in fibrillatory wavefronts across all layers.

The data shows that extending the substrate from a single layer to a double layer grid results in the transition point falling from $\nu = 0.143 \pm 0.002$ to 0.098 ± 0.002 . The main sources of error in these results are the resolution at which data was collected and the parameter fitting of the curve from which the steepest point is calculated. This change suggests that adding a second layer makes the system more stable as it is more difficult for critical structures to form at values of ν between 0.098 and 0.143 ± 0.002 . This is likely due to the fact that the presence of a second layer gives the signal more opportunities to bypass a defective cell without forming a re-entry circuit.

The single layer model is thus a special case. As shown in Figure 4.3, as the number of layers is increased to values higher than 2, the steepest point of the transition also rises. Fibrillation occurs at higher values of ν for multiple layers: effectively, a larger number of layers results in a less stable substrate. Figure

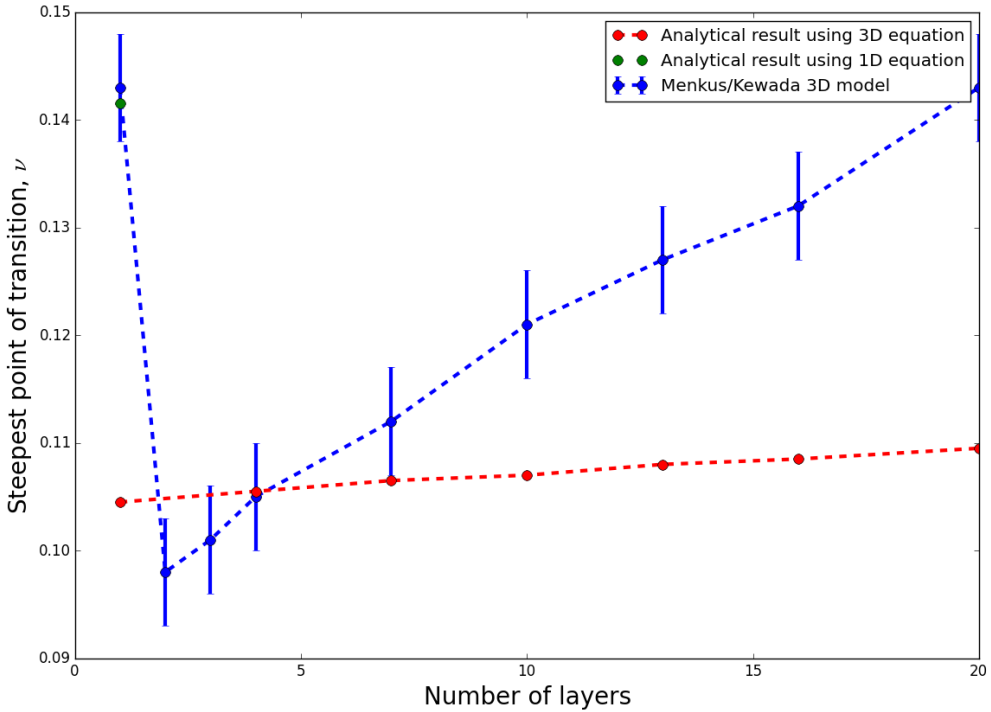


Figure 4.3: Graph showing the steepest transition point for simulations of different number of layers. The analytical result given by Equations 2.4 and 2.5 are plotted for comparison.

4.3 also shows the analytical result calculated using Equation 2.4 for the single layer case and Equation 2.5 for the many layer substrate. As evident in Figure 4.3, the simulation showed a more pronounced trend of increasing transition point than the analytical result predicted. There are 3 possible suppositions which explain this disparity.

The most likely cause of the disparity are the assumptions under which the analytical result was calculated. Equations 2.4 and 2.5 identify P_{risk} : the probability of developing atrial fibrillation in a simulation. The data collected from the model gives the risk of fibrillation occurring as the time spent in fibrillation, divided by the total time and averaged over the number of simulations. Thus, the equalities given by Equations 4.1 and 4.2 is assumed despite not being generally true.

$$P_{risk} = \left\langle \frac{T_{af}}{T_{tot}} \right\rangle \quad (4.1)$$

Equation 4.2 can also be written as:

$$P_{risk} = \frac{N_{af}}{N} = \frac{N(1c.s.)}{N} = \frac{1}{N} \sum_{i=0}^N \frac{T_{af}^{(i)}}{T} \quad (4.2)$$

Where N_{af} is the number of simulations in which fibrillation occurred and N is the total number of simulations. Thus N_{af} is equivalent to the number of simulations in which there was at least 1 critical structure, $N(1c.s.)$. The final term denotes the method used to calculate P_{risk} from the simulations, where $T_{af}^{(i)}$ is the time simulation i spent in fibrillation, and T is the total time of the simulation. The final equality is thus only true in the $\lim_{N \rightarrow \infty}$ and $\lim_{T \rightarrow \infty}$. That is, the analytical result assumes that if a given simulation experiences AF at all, then that AF is persistent and comprises the entire length of the simulation. This is only true when the total time of the simulation is extremely long. Moreover, the assumption that all fibrillation is persistent discounts the effect of paroxysmal events. This is of particular significance to Figure 4.3 because is in the range of the values of ν at which the transition occurs that paroxysmal events occur most frequently. This hypothesis could be verified by optimizing the model to allow for much longer simulations

to be run and by recording the number of AF events and their lengths.

The second and third reasons for the disparity in Figure 4.3 are both higher order effects that the analytical solution does not take into account, namely, effects caused by rotors interacting and the more complex critical structures. The ability for wavelets from a rotor to ignite a second rotor is demonstrated in Figure 4.4. Christensen *et al*'s analytical solution does not need to take this effect into account as it is irrelevant during persistent fibrillation and the solution assumes all fibrillation to be persistent. However, this effect is significant in increasing the number of paroxysmal events, and it is a phenomenon that scales with system size, making it particularly relevant in the 3D model.

Moreover, visualisations showed that multiple rotors can interact and depending upon their phase difference, have the ability to terminate or perpetuate a fellow rotor. The phase difference of rotors is a function of both the length of the rotors and their position relative to one another, making it a highly complex phenomenon.

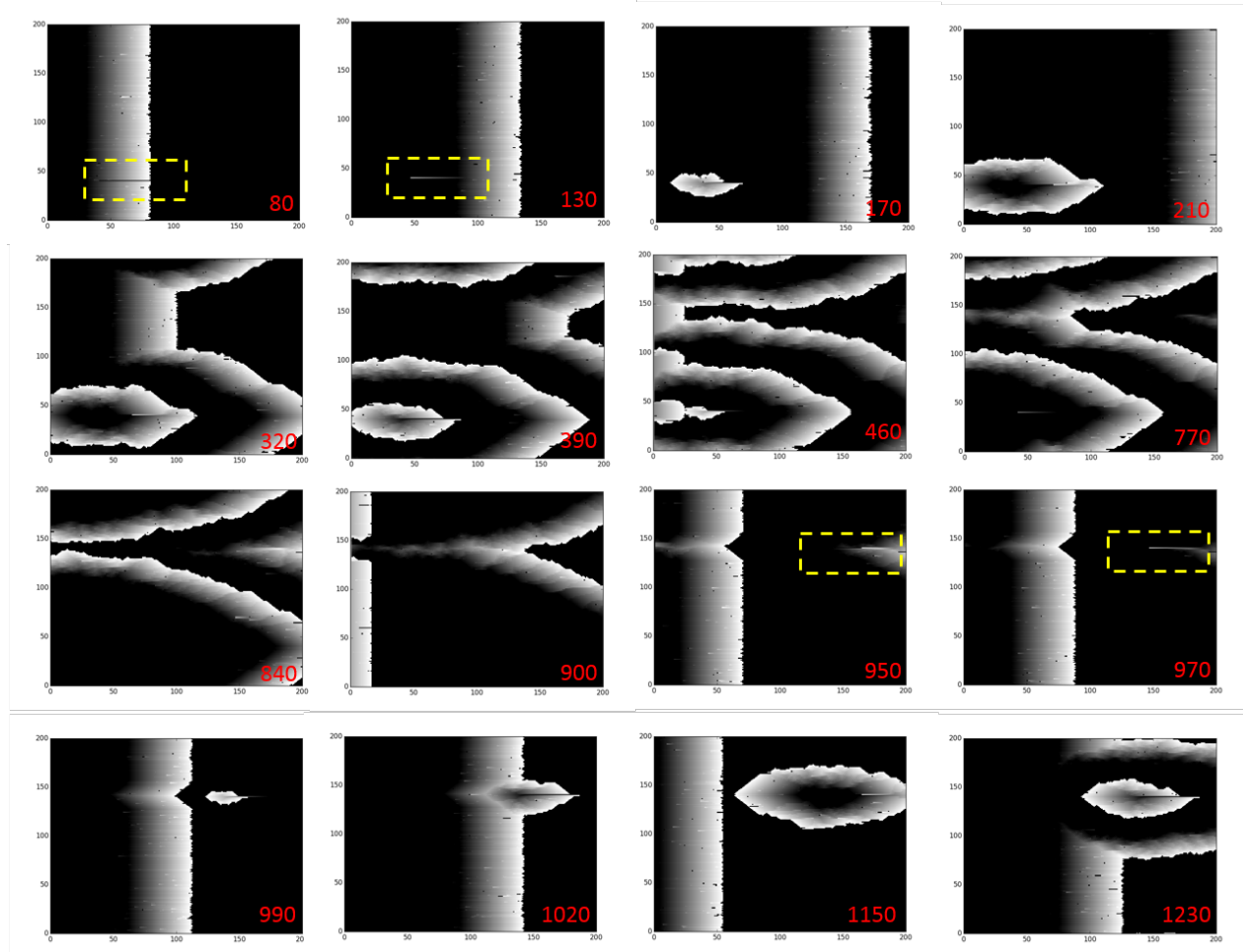


Figure 4.4: Screenshots from visualisation showing wavelets from a rotor igniting a second rotor. The timestamp of the image is given on red in the bottom right corner of each screenshot. A rotor is shown forming in the bottom left corner of the grid at $T=80$, outlined in yellow hashing. This results in fibrillatory behaviour which begins to die out and in doing so, ignites a second rotor as shown in $T=950$ and $T=970$. Timestamps are given for relative comparison.

The final possible explanation for Figure 4.3's disparity is that the analytical solution does not include the probability of more complex critical structures forming.

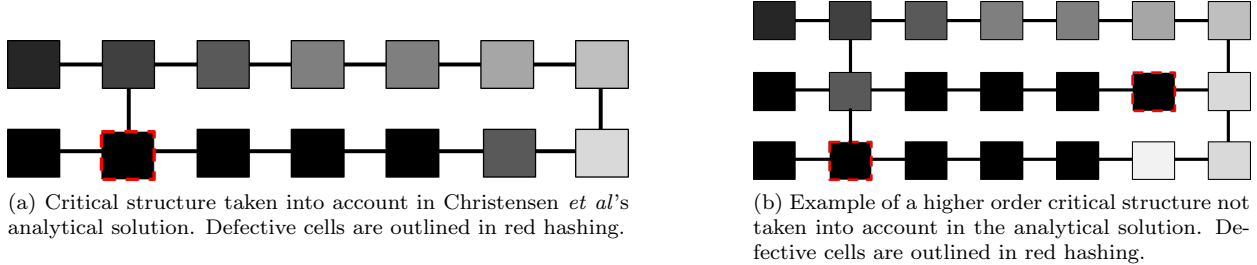


Figure 4.5

4.2 Anatomical Model Results

Sinus rhythm in the Anatomical model is pictured in Figure 4.6. The signal can be seen originating from the pacemaker cells (Figure 4.6 [1]) and propagating over the heart in a quasi-wavefront. The uneven wavefront is caused by both the fibre orientation and defective cells.

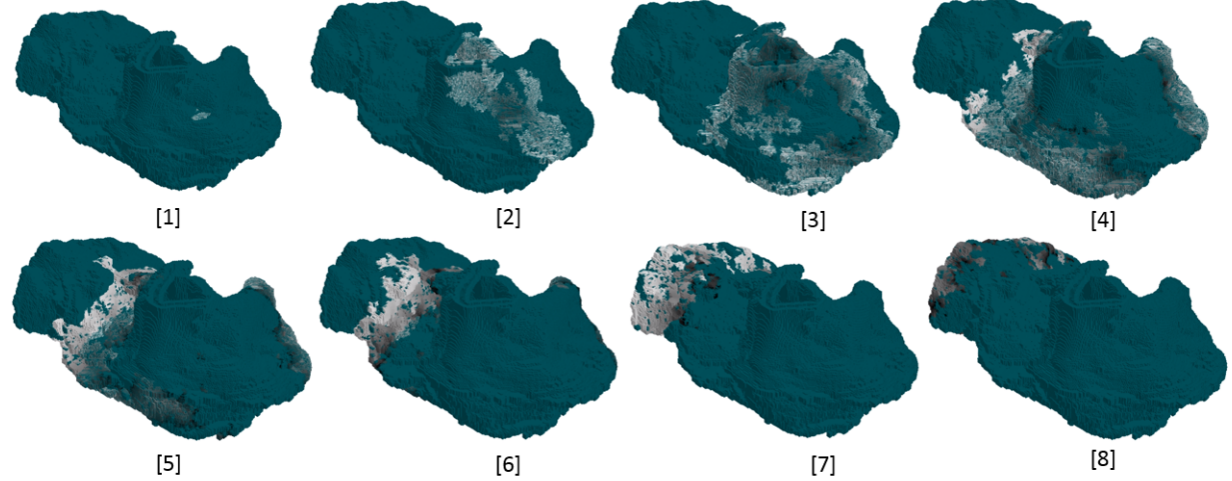
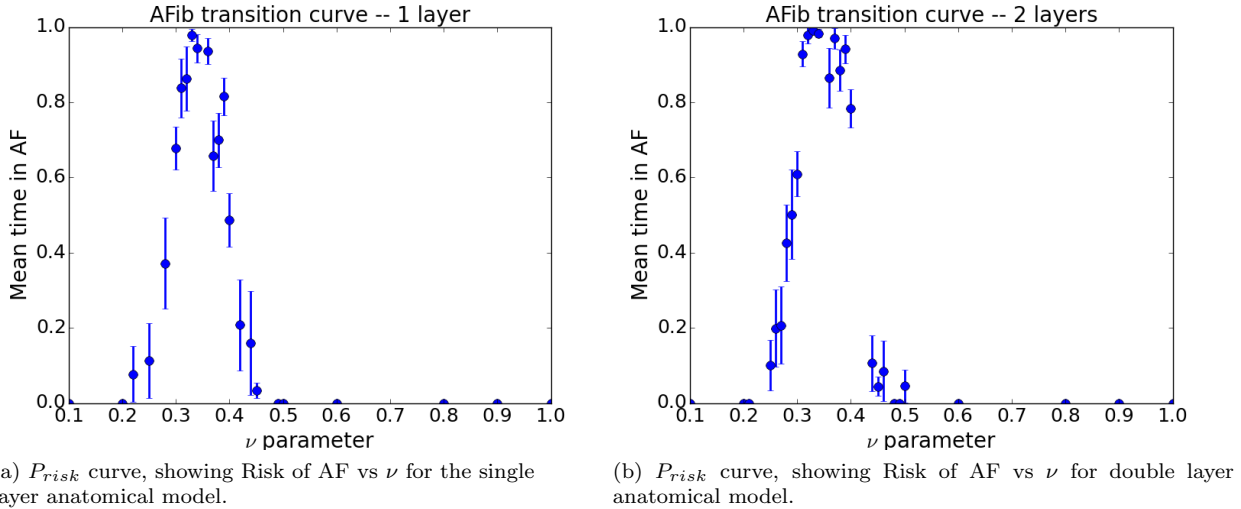


Figure 4.6: Visualisation of right atrium in the Anatomical Model showing sinus rhythm. Excited cells are pictured in white and refractory in progressive shades of grey. Images taken between 0 and 5000 timesteps at intervals of 500 timesteps.

4.2.1 Transition curve relationship

The Anatomical model was shown to preserve the transition relationship between ν and AF Risk given by the Christensen *et al* model. Figure 4.7a shows the risk of atrial fibrillation at different values of ν for simulations run on a single layer dataset, where each data point is the median time spent in fibrillation across a minimum of 10 simulations. It shows a transition point of $\nu = 0.38 \pm 0.01$, below which the risk of atrial fibrillation increases sharply to 1. This value is significantly higher than the transition point value 0.143 ± 0.01 of the 2D model, suggesting that atrial fibrillation forms at higher values of ν when a realistic topology and fibre orientation is taken into account. Heuristically, this result is expected: the geometry and fibre orientation add a greater level of inhomogeneity into the system and one would expect the risk of fibrillation to increase as a result.

Futhermore, Figure 4.7a shows that at values of ν below 0.24 ± 0.03 , the risk of fibrillation falls to zero, a result of full conduction across the surface not being possible at such low connectivity. The error is given by interpolation between results, and is limited by the resolution of ν at which datapoints were taken. It was surmised that this was the result of running the simulation on a single layer of cells. Whilst



fibrillation is a mostly surface effect, the fibre connectivity is inherently three dimensional and thus taking just a single layer of cells is artificial and likely to result in areas of the atrium which are disconnected (particularly if their fibre vectors are approximately perpendicular to the surface). It was postulated that this effect would be reduced if the simulation was run on several layers instead.

Figure 4.7b shows the transition relationship between ν and risk of fibrillation for simulations run on 2 layers of the anatomical model. The steepest point of the transition, below which the risk of atrial fibrillation becomes 1 is at $\nu = 0.42 \pm 0.01$. This is higher than the transition value for the simulation of a single layer in the anatomical model. The 3D Cylindrical model showed that as the number of layers is increased from 1 to 2, the value of the transition point drops, however, increasing the number of layers beyond 2 results in a systematic increase in the transition value. The Anatomical model shows an increased transition from 1 to 2 layers, a difference from the 3D Cylindrical model that is due to the fibre orientation. The lowest value of ν which supports conduction on the 2 layer anatomical model is 0.23 ± 0.02 , marginally lower than that of the 1 layer model. Thus increasing the number of layers did not increase the minimum conduction point in a significant manner.

4.2.2 New Phenomena

Atrial fibrillation was observed as occurring in two separate modes with different causal triggers. The first mode of fibrillation emerged from the development of re-entrant circuits on the surface of the atrium. These rotors were observed to be transient: they would often terminate within the course of a simulation and multiple rotors were often observed at the same point in time. It is likely that the probability of the first rotor forming is lower than the probability of the second circuit forming and that of every additional rotor after that. This is due to the fact that the first rotor results in the creation of multiple excitatory wavelets, making it more likely for critical structures to receive their triggering excitation. These re-entrant circuits were similar to those seen in the 2D Christensen *et al* model, and thus qualitatively support the original findings.

The second mode of AF observed was that which occurred without the presence of re-entrant circuits. The fibrillatory behaviour was instead caused by multiple wandering wavelets, as shown in Figure 4.8. This was a new phenomenon, previously unseen in the Christensen *et al* model. It is generally observed to occur in a smaller range of values of ν , at the lower end of the range that supports fibrillation caused by rotors. These wandering wavelets are pictured in Figure 4.8. These observations are consistent with Moe's multiple wavelet hypothesis. Moe formed this hypothesis based on data from a simple cellular automata model similar to that of Christensen *et al*. He hypothesised that fibrillation is maintained by the "irregular wandering of numerous wavelets generated by the fractionation of a wavefront passing through tissue in a state of inhomogeneity" [15]. Moe proposed a number of biological sources of these inhomogeneities, including structural inhomogeneities and the variation of the refractory period over the atrial area. The results from the anatomical model suggests that the fibre orientation is a factor that increases the heterogeneity, thereby increasing the probability of such wavelets forming. Thus the model proposes a new source of structural inhomogeneity that explains the formation of these wavelets.

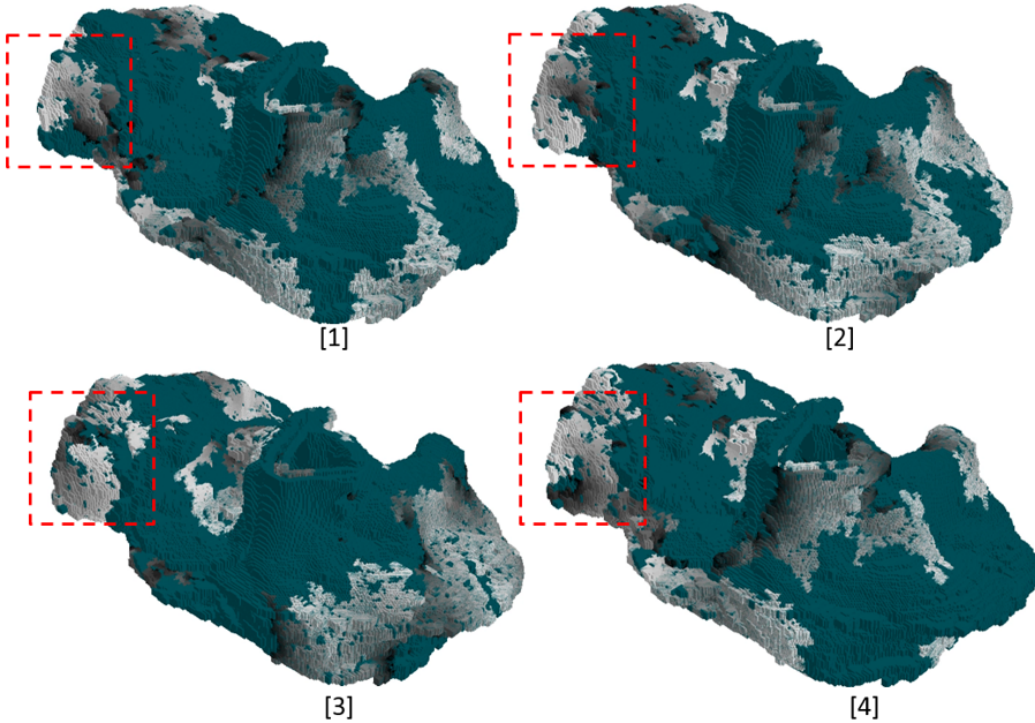


Figure 4.7: Visualisations of a simulation showing fibrillation across the atrium. The triggering rotor, forming a characteristic spiral, has been highlighted with red hashing. Simulation run at $\nu = 0.38$. Images taken at consecutive timesteps of $t=50$.

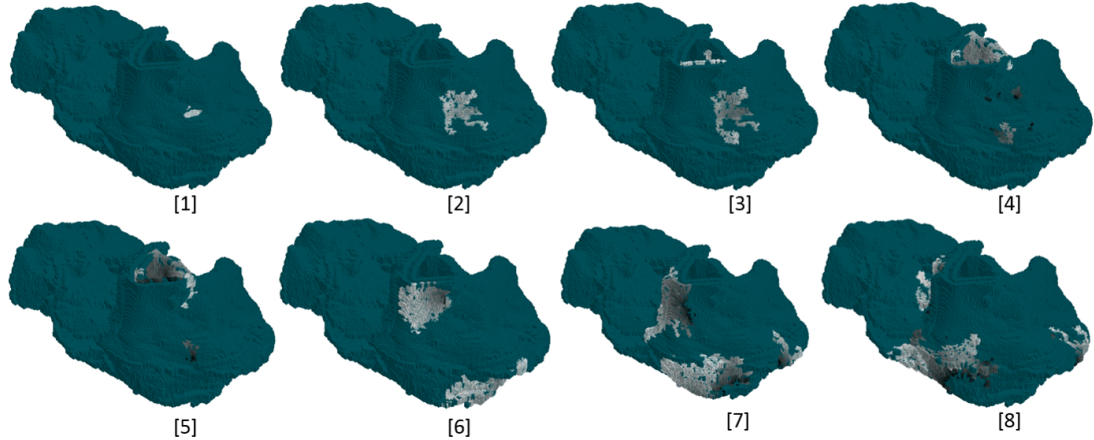
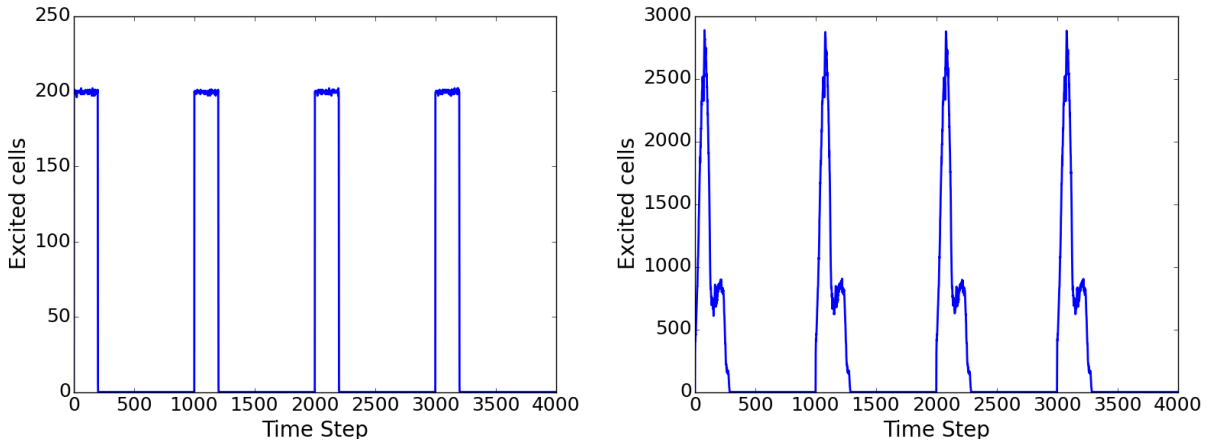


Figure 4.8: Visualisations of a simulation showing fibrillation across the atrium in the form of multiple wandering wavelets. Simulation run at $\nu = 0.33$. Images taken at consecutive timesteps of $t=10$.

The electrocardiograms given by the Anatomical model differ significantly from those of the Christensen *et al* model during sinus rhythm. In the anatomical model sinus rhythm does not resemble the square wave pattern produced by the Christensen *et al* model, but instead has a more realistic spiking characteristic, as shown in Figure 4.9.

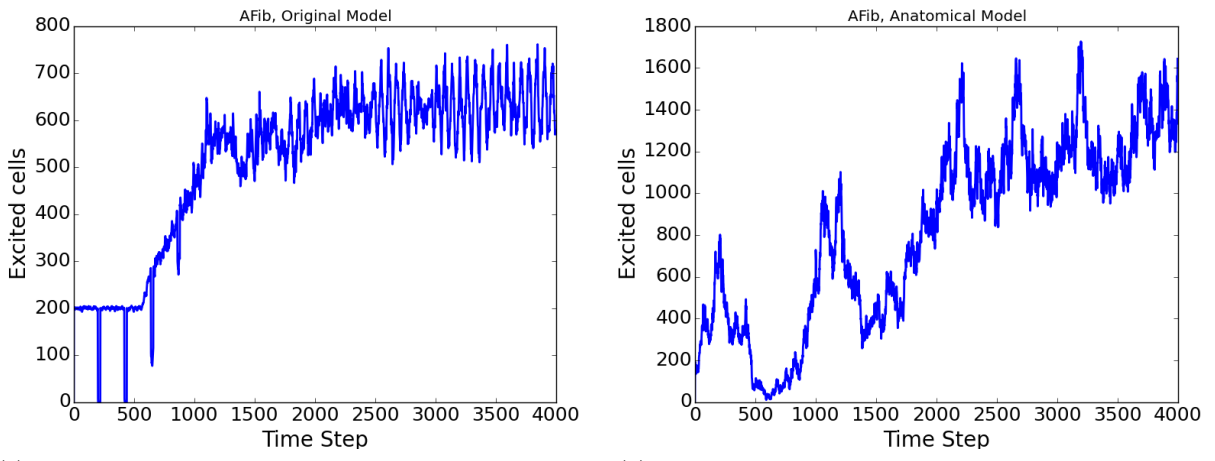
As shown in Figure 4.10 the electrocardiograms the Anatomical model shows the same characteristic irregularity as that from the Christensen *et al* model. However in Anatomical model it occurs over a wider range of number of excited cells, a direct result of the 2 different causes of AF. This is shown in Figure 4.10b:



(a) Graph showing the number of excited cells with time during sinus rhythm in the Christensen *et al* model.

(b) Graph showing the number of excited cells with time during sinus rhythm in the Anatomical model.

Figure 4.9: Comparison of the electrocardiograms from the Christensen *et al* model and the Anatomical model during sinus rhythm. Taken at $\nu = 0.8$.



(a) Graph showing the number of excited cells with time during AF in the Christensen *et al* model.

(b) Graph showing the number of excited cells with time during AF in the Anatomical model.

Figure 4.10: Comparison of the electrocardiograms from the Christensen *et al* model and the Anatomical model during AF. Taken at $\nu = 0.13$ and 0.33 respectively.

the fibrillation occurring at lower numbers of excited cells (between 0 and 1500 timesteps) is the result of wandering wavelets, whilst that occurring after 2500 was observed to be the result of a rotor forming in the substrate.

4.3 Event Lifetime Results

As shown in Figure 4.11 the Markov Chain analysis correctly describes a linear relationship between $\frac{1}{\epsilon}$ and median event lifetime, however, it consistently underpredicts it. This systematic discrepancy is due to the fact that the analytical solution given by Markov chain analysis predicts the rotor lifetime, whereas the data from the simulation represents the median AF event lifetime. It is evident that both trends show strong linear correlation, with $r=0.999$ for the analytical solution and $r=0.987$ for the data from the model. The

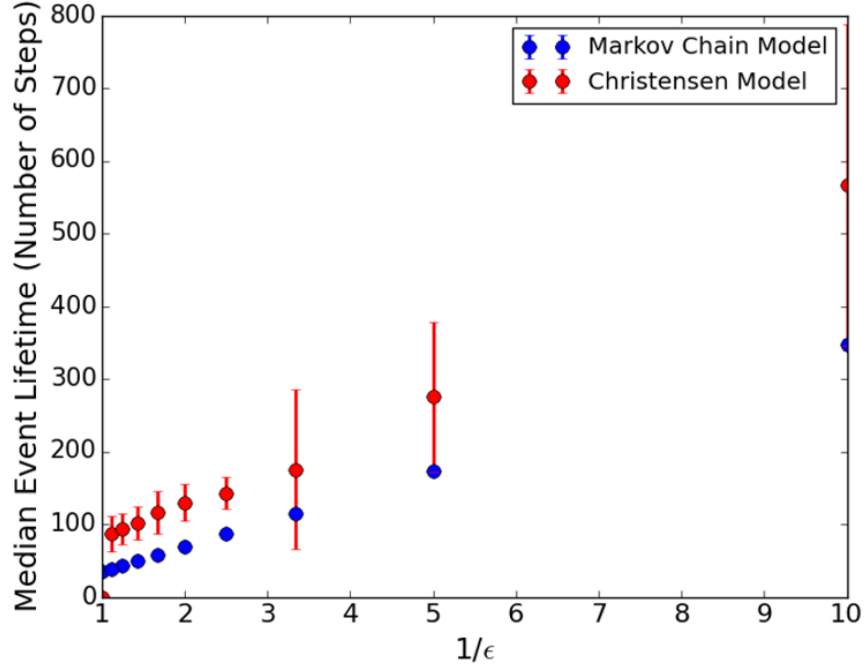


Figure 4.11: Graph comparing data from simulations and the analytical Markov Chain results for the relation between $\frac{1}{\epsilon}$ and event lifetime.

error from the simulation was calculated as the interquartile difference. Errors calculated on the analytical solution are negligible and therefore not visible in Figure 4.11. Histograms were generated for each datapoint in Figure 4.11, showing the distribution of the dataset whose median is plotted above. This showed that the data, even in the limit of a large number of trials, is not Gaussian and instead is often bi-modal: a characteristic which would increase the errors given on the datapoints.

Chapter 5

Conclusion

Atrial fibrillation is a prevalent arrhythmic condition that is not well understood. A number of computer models have been developed to this end, including a simple cellular automata model by Christensen *et al* that provided a causal link between fibrosis in patients and the emergence of atrial fibrillation. This simple, discretised model was successfully applied to an atrial geometry with realistic fibre orientations, thereby creating a hybrid model with the efficiency of a cellular automata and the anatomical data of a geometric model. Image based data from a sheep's atrium was acquired, and significant data processing was undertaken to discretize the physiological data. This Anatomical model was implemented in 3 dimensions with each cell having a maximum of 18 possible connections to its neighbours. Extensive optimization was carried out to obtain a realistic run time for the model. The Anatomical Model was shown to preserve the statistical behaviour seen in the Christensen *et al* model, in particular the sharp transition relationship between the transverse coupling, ν , and the risk of AF. The model did result in new mechanisms for AF to develop, as fibrillation was shown to occur without rotors but instead as the result of wandering wavelets arising from the heterogeneic connectivity of the fibre orientation, validating a hypothesis given by Moe in 1964.

A 3D model was created by coupling together 2D sheets of the original Christensen *et al* model. The 3D geometry was shown to preserve the transition relationship between ν and risk of AF but increasing the number of layers was shown to shift the transition, making the system less stable. The model also showed high levels of heterogeneity between layers, validating the hypothesis that atrial fibrillation acts effectively as a surface phenomenon and thus can be modelled as such.

5.1 Further Developments

With the anatomical model fully implemented, a number of areas present themselves for further investigation. However, the anatomical model may initially require further optimisation, such that it can be run using the entire dataset of the atrium rather than just a few layers. The purpose of this is twofold: it will allow for the a phenomenon known as 'epi-endo dissociation' to be investigated and it will also make the model extremely time efficient when run on a desktop computer, a factor particularly important for future clinical applications.

Epi-endo dissociation requires a volumetric model to be simulated. Traditionally, simulations of AF assumed that whilst the atrium is 3 dimensional, the difference in activation time between the epicardium and the atrial free walls are small. This allows for the atrium to effectively be treated as a 2 dimensional surface on which fibrillating waves propagate [28]. However recent investigations using both computational modeling and clinical studies on goats hearts have shown that over time persistent atrial fibrillation leads to increased dissociation between the epicardial and endocardial layer, as a result of fibrosis [29]. As a result, 'breakthrough' waves are observed in the epicardium, increasing the complexity of the fibrillatory behaviour and suggesting that atrial fibrillation is in fact a 3 dimensional problem. As such, the Anatomical model would be ideal for modelling this dissociation and its effects or progression over time.

Additional developments include using the model to investigate treatment procedures of AF. Treatments such as the Maze procedure, in which a number of strategically placed incisions are made across the atrial wall causing it to form scar tissue thus disrupting the paths of abnormal electrical activity, require a geometrically accurate model.

Chapter 6

Appendix

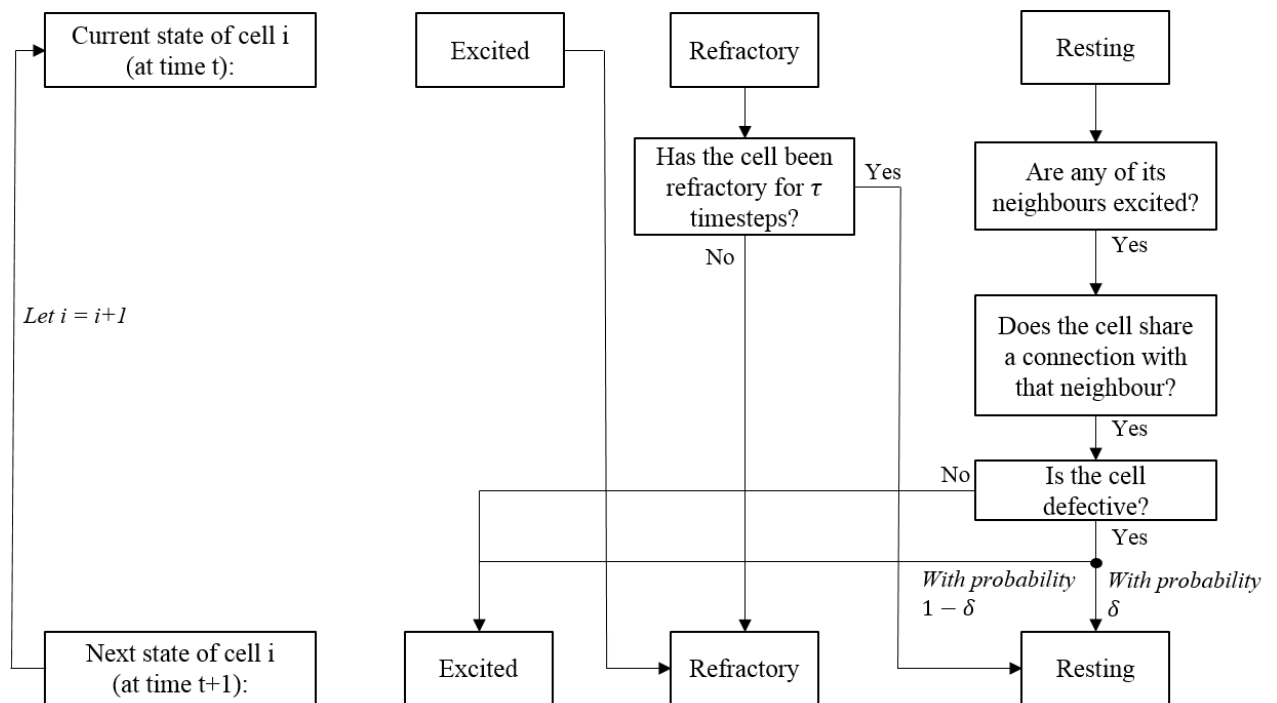


Figure 6.1: Flow diagram showing the algorithm governing the 2D Christensen *et al* model. This process used to update the state of a cell from timestep t to $t+1$ and is repeated for every cell in the grid.

Bibliography

- [1] Hart, R. G., & Halperin, J. L. (2015). Comments, Opinions, and Reviews, 803808.
- [2] Chugh, S. S., Havmoeller, R., Narayanan, K., Singh, D., Rienstra, M., Benjamin, E. J., Murray, C. J. L. (2014). Worldwide Epidemiology of Atrial Fibrillation: A Global Burden of Disease 2010 Study. *Circulation*, 129(8), 837847. doi:10.1161/CIRCULATIONAHA.113.005119
- [3] Nattel, S. (2002). New ideas about atrial fibrillation 50 years on. *Nature*, 415(6868), 219226. doi:10.1038/415219a
- [4] Hall, J. E. (2011) Guyton and Hall Book of Medical Physiology 13th Edition, pp. 165
- [5] Sutter Health. (2014) Atrial Fibrillation - Information, Symptoms, Treatment Options Sutter Health CMPC website, visited [24/04/2016]
- [6] Klabunde, R. E. (2005) Cardiovascular Physiology Concepts Lippincott Williams and Wilkins, pp. 43
- [7] Sommer, J., Dolber, P. Cardiac muscle: ultrastructure of its cells and bundles Normal and Abnormal Conduction in the Heart p. 1-27
- [8] Manani, K. (2015). A Cellular Automata Model for Identifying Critical Structures in Atrial Fibrillation Late Stage Assessment Report, Imperial College London
- [9] Plonsey, R., Barr, R. C. (2007) Bioelectricity, A Quantitative Approach Springer, p.97-99.
- [10] UTAS, Cardiovascular Tissue Index School of Medicine, Discipline of Pathology website visted [24/04/2016]
- [11] Bullock, TH; Orkand, R; Grinnell, A (1977). Introduction to Nervous Systems. W. H. Freeman. p. 151.
- [12] Lawhon, B. (2013)
<http://wesleytodd.blogspot.com/2013/11/action-potentials.html>
- [13] Marban, E. (2002). Cardiac channelopathies. *Nature*, 415(January), 213218. doi:10.1038/415213a
- [14] Nattel, S. (1998). Experimental evidence for proarrhythmic mechanisms of antiarrhythmic drugs. *Cardiovascular Research*, 37(3), 56777. doi:10.1016/S0008-6363(97)00293-9
- [15] Moe, G., Rheinboldt, W., Abildskov, J. (1964) A computer model of atrial fibrillation Am. Heart J
- [16] Allessie, M., Lammers, W., Bonke, F., Hollen, J. (1985) Experimental evaluation of Moe's multiple wavelet hypothesis of atrial fibrillation Cardiac electrophysiology and arrhythmias
- [17] Mansour, M., Mandapati, R., Berenfeld, O., Chen, J., Samie, F. H., & Jalife, J. (2001). Left-to-right gradient of atrial frequencies during acute atrial fibrillation in the isolated sheep heart. *Circulation*, 103(21), 26312636. doi:10.1161/01.CIR.103.21.2631
- [18] Keener, J., Sneyd, J. (2009) Mathematical Physiology I: Cellular Physiology Springer, p.197-223 .
- [19] Trayanova, N. a. (2014). Mathematical Approaches to Understanding and Imaging Atrial Fibrillation: Significance for Mechanisms and Management. *Circulation Research*, 114(9), 15161531. doi:10.1161/CIRCRESAHA.114.302240
- [20] Zhao, J., Butters, T. D., Zhang, H., Legrice, I. J., Sands, G. B., & Smaill, B. H. (2013). Image-based model of atrial anatomy and electrical activation: A computational platform for investigating atrial arrhythmia. *IEEE Transactions on Medical Imaging*, 32(1), 1827. doi:10.1109/TMI.2012.2227776
- [21] McDowell, K. S., Vadakkumpadan, F., Blake, R., Blauer, J., Plank, G., MacLeod, R. S., & Trayanova, N. a. (2013). for patient-specific modeling of atrial fibrosis as a substrate for atrial fibrillation, 18(9), 11991216. doi:10.1016/j.jelectrocard.2012.08.005.Methodology

- [22] Christensen, K., Manani, K. a., & Peters, N. S. (2015). Simple Model for Identifying Critical Regions in Atrial Fibrillation. *Physical Review Letters*, 114(2), 028104. doi:10.1103/PhysRevLett.114.028104
- [23] van der Schaaf, A., Langendijk, J., Fiorino, C., Rancati, T. (2015) Embracing Phenomenological Approaches to Normal Tissue Complication Probability Modeling: A Question of Method. *International Journal of Radiation Oncology*Biology*Physics*, Volume 91, Issue 3.
- [24] Manani, K. (2015). A Cellular Automata Model for Identifying Critical Structures in Atrial Fibrillation Supplementary Materials, Imperial College London
- [25] Bub, G., & Shrier, A. (2002). Propagation through heterogeneous substrates in simple excitable media models Chaos: An Interdisciplinary Journal of Nonlinear Science, 12(3), 747. doi:10.1063/1.1502481
- [26] CIZ Anatomy Zone Encyclopedia (2015) Image taken from online encyclopedia, visited [24/04/2016]
- [27] Greenberg, J. M., & Hastings, S. P. (1978). Spatial Patterns for Discrete Models of Diffusion in Excitable Media. *SIAM Journal on Applied Mathematics*, 34(3), 515523. doi:10.1137/0134040
- [28] Verheule, S., Eckstein, J., Linz, D., Maesen, B., Bidar, E., Gharaviri, A., & Schotten, U. (2014). Role of endo-epicardial dissociation of electrical activity and transmural conduction in the development of persistent atrial fibrillation. *Progress in Biophysics and Molecular Biology*, 115(2-3), 173185. doi:10.1016/j.pbiomolbio.2014.07.007
- [29] Verheule, S., Tuyls, E., Gharaviri, A., Hulsmans, S., Hunnik, A. Van, Kuiper, M., Zeemering, S. (2016). Loss of Continuity in the Thin Epicardial Layer Because of Endomyocardial Fibrosis Increases the Complexity of Atrial Fibrillatory Conduction. doi:10.1161/CIRCEP.112.975144